Structural Dichotomy in Six-Coordinate d^0 Complexes: Trigonal Prismatic $(^tBu_3SiC{\equiv}C)_6Ta^-$ and Octahedral $(^tBu_3SiC{\equiv}C)_6M^{2-}$ (M = Zr, Hf)

Thomas P. Vaid,[†] Adam S. Veige,[†] Emil B. Lobkovsky,[†] Wingfield V. Glassey,[†] Peter T. Wolczanski,*[,†] Louise M. Liable-Sands,[‡] Arnold L. Rheingold,[‡] and Thomas R. Cundari[§]

Contribution from the Department of Chemistry & Chemical Biology, Baker Laboratory, Cornell University, Ithaca, New York 14853, Department of Chemistry, University of Delaware, Newark, Delaware 19716, and Department of Chemistry, University of Memphis, Memphis, Tennessee 38152

Received January 26, 1998

Abstract: Utilization of the bulky acetylide, $^tBu_3SiC{\equiv}C^-$, enabled the synthesis of several early metal polyacetylides. Addition of $NaC{\equiv}CH$ to $^tBu_3SiBr$ in dimethyl sulfoxide afforded $^tBu_3SiC{\equiv}CH$, which was deprotonated to yield $^tBu_3SiC{\equiv}CLi$. Treatment of $ZrCl_4$, $HfCl_4$, and $TaCl_5$ with varying amounts of $^tBu_3SiC{\equiv}CLi$ gave $\{(THF)_2Li(^tBu_3SiC{\equiv}C)_2\}Zr(C{\equiv}CSi^tBu_3)_3(THF)$ (**1**; THF = tetrahydrofuran), $\{(Et_2O)Li(^tBu_3SiC{\equiv}C)_2\}Hf(C{\equiv}CSi^tBu_3)_3(OEt_2)$ (**2**), $\{Li(^tBu_3SiC{\equiv}C)_3\}_2M$ (M = Zr, **6**; Hf, **7**), and $\{Li(^tBu_3SiC{\equiv}C)_3\}Ta(C{\equiv}CSi^tBu_3)_3$ (**3**). Metathesis of **3** with KOTf generated $KTa(C{\equiv}CSi^tBu_3)_6$ (**4**) and cation sequestration of **4** with crypt 2.2.2 provided $[K(crypt\ 2.2.2)][Ta(C{\equiv}CSi^tBu_3)_6]$ (**5**). Single-crystal X-ray structural studies determined the structures (core symmetry) of **1** (O_h), **2**, (O_h), **3** (D_3), **5** (D_3), **6** (O_h), and **7** (O_h). The D_{3h} to D_3 twist in **3** and **5** has a steric origin, and the counterion position appears inconsequential. Origins of the structural preferences illustrated by the dichotomous twisted trigonal prismatic and octahedral cores of the d^0 hexaacetylides **5** and **6** were probed through density functional (ADF) and effective core potential (GAMESS) calculations. The structural difference results from a lessening electronic preference for the trigonal prism—primarily a greater HOMO/LUMO gap—upon moving from Ta to Zr, minor steric factors, and increased interligand repulsions in the dianion (VSEPR).

Introduction

Until recently, any six-coordinate d^0 complex, MX_6^{n-} (X is monodentate), would be assigned an octahedral structure according to the valence shell electron pair repulsion (VSEPR) model.[1] This paragon was challenged by Kang, Albright and Eisenstein,[2−4] who postulated that distortions to trigonal prismatic (D_{3h}) or even lower (e.g., C_{3v}) symmetry were plausible for nonbulky ligands with little or no π-bonding capability. Calculations revealed that a lowering of symmetry from O_h enabled ligand-localized, filled σ-orbitals (HOMO) to mix with empty, π-type orbitals (LUMO) in a d^0 system, resulting in significant stabilization, at least for the hypothetical MH_6^{n-} derivatives upon which the first computational studies were based. While these efforts were greeted with some initial skepticism from experimentalists, vindication was achieved via the structural confirmation of trigonal prismatic $[ZrMe_6]Li_2(tmeda)_2$ (tmeda = *N*,*N*,*N*′,*N*′-tetramethylethylenediamine) by Morse and Girolami,[5] and Wilkinson's distorted trigonal prismatic WMe_6.[6] WMe_6 was proposed to be a trigonal prism on the basis of Haaland's electron diffraction study,[7] but clarification of further distortion was ultimately obtained through the greater resolution of a single-crystal X-ray diffraction investigation by Pfennig and Seppelt.[8] Density functional theory (DFT) calculations by Kaupp[9] augmented the structural investigations of WMe_6 by predicting these distortions and effectively reiterating previous calculational assessments.

During the course of investigation into possible syntheses of met-cars,[10] alkynyl ligands were considered a source of dicarbide, C_2^{4-},[11] but difficulties were encountered in preparing polyalkynyl derivatives of several early metal halides. For example, treatment of Cp^*ZrCl_3 ($Cp^* = \eta^5$-C_5Me_5)[12] with 3 equiv

[†] Cornell University.
[‡] University of Delaware.
[§] University of Memphis.

(1) (a) Gillespie, R. J.; Hargittai, I. *The VSEPR Model of Molecular Geometry*; Allyan and Bacon: Boston, 1991. (b) Gillespie, R. J.; Nyholm, R. S. *Q. Rev. Chem. Soc.* **1957**, *11*, 339−380.
(2) Kang, S. K.; Tang, H.; Albright, T. A. *J. Am. Chem. Soc.* **1993**, *115*, 1971−1981.
(3) Kang, S. K.; Albright, T. A.; Eisenstein, O. *Inorg. Chem.* **1989**, *28*, 1611−1613.
(4) Demolliens, A.; Jean, Y.; Eisenstein, O. *Organometallics* **1986**, *5*, 1457−1464.
(5) Morse, P. M.; Girolami, G. S. *J. Am. Chem. Soc.* **1989**, *111*, 4114−4116.
(6) (a) Shortland, A. J.; Wilkinson, G. *J. Chem. Soc., Dalton Trans.* **1973**, 872−876. (b) Calyer, A. L.; Wilkinson, G. *J. Chem. Soc., Dalton Trans.* **1976**, 2235−2238.
(7) Haaland, A.; Hammel, A.; Rypdal, K.; Volden, H. V. *J. Am. Chem. Soc.* **1990**, *112*, 4547−4559.
(8) Pfennig, V.; Seppelt, K. *Science* **1996**, *271*, 626−628.
(9) Kaupp, M. *J. Am. Chem. Soc.* **1996**, *118*, 3018−3024.
(10) (a) Guo, B. C.; Kearns, K. P.; Castleman, A. W. *Science* **1992**, *255*, 1411−1413. (b) Guo, B. C.; Wei, S.; Purnell, J.; Buzza, S.; Castleman, A. W. *Science* **1992**, *256*, 515−516. (c) Wei, S.; Guo, B. C.; Purnell, J.; Buzza, S.; Castleman, A. W. *Science* **1992**, *256*, 818−820. (d) Cartier, S. F.; Chen, Z. Y.; Walder, G. J.; Sleppy, C. R.; Castleman, A. W. *Science* **1993**, *260*, 195−196.
(11) Hoffmann, R. *Angew. Chem., Int. Ed. Engl.* **1988**, *27*, 1593−1602.

S0002-7863(98)00289-3 CCC: $15.00
Published on Web 09/19/1998

of $LiC{\equiv}CSiMe_3$ resulted in an intractable mixture, whereas Cp^*ZrR_3 (R = Me, CH_2Ph, Ph,[12] etc.) are readily prepared via related routes. While there are many examples of $Cp_2M(CCR)_2$ (Cp = η^5-C_5H_5 or η^5-C_5H_4R, etc.; M = Ti, Zr, Hf),[13,14] few cases of an early transition metal bound to more than two alkynyl ligands are known (e.g., $\{Li(TMEDA)_2\}[V(C{\equiv}CPh)_4]$-(tmeda)).[15,16] Since homoleptic hydrocarbyls have historically been considered critical synthetic targets,[13] the paucity of relevant early metal examples may be construed as a testament to the reactivity of the alkynyl functional group. Side reactions, such as insertion of the C$\alpha{\equiv}$Cβ unit,[17] external $RC{\equiv}C^-$ attack at Cα or Cβ,[13,14] and dinuclear reductive elimination[18-20] may interfere with standard metathetical routes and terminal alkynyl stability.

Use of the Si^tBu_3 group enabled the synthesis of unusual, low-coordinate early metal derivatives such as $Ta(OSi^tBu_3)_3$,[21] $Ti(OSi^tBu_3)_3$,[22] and $(^tBu_3SiO)_2W{=}N^tBu$,[23] prompting the extension of this steric protecting group[24] to alkynyl chemistry. The successful utilization of $^tBu_3SiC{\equiv}C$ in the synthesis of alkynyl derivatives of Zr, Hf, and Ta is reported herein, along with the discovery of a structural dichotomy for six-coordinate, homoleptic d^0 derivatives: trigonal prismatic $(^tBu_3SiC{\equiv}C)_6Ta^-$ and octahedral $(^tBu_3SiC{\equiv}C)_6M^{2-}$ (M = Zr, Hf).

Results

Synthesis of $HC{\equiv}CSi^tBu_3$ and $LiC{\equiv}CSi^tBu_3$. Treatment of $^tBu_3SiBr$[25] with $NaC{\equiv}CH$ (or $MgBrC{\equiv}CH$) in tetrahydrofuran (THF) resulted in no reaction, even at elevated temperatures, but use of dimethyl sulfoxide (DMSO) as solvent afforded $^tBu_3SiC{\equiv}CH$ and $^tBu_3SiC{\equiv}CSi^tBu_3$ in an ~8:1 ratio over a period of 13 days at 22 °C (eq 1). Attempts to speed the reaction by elevating the temperature resulted in the almost

$$^tBu_3SiBr + NaC{\equiv}CH \xrightarrow[-NaBr,\ -C_2H_2]{DMSO,\ 22\ ^\circ C,\ 14\ days} {}^tBu_3SiC{\equiv}CH + {}^tBu_3SiC{\equiv}CSi^tBu_3 \quad (1)$$

exclusive production of $^tBu_3SiC{\equiv}CSi^tBu_3$. Partial dissolution of the mixture in a minimal amount of acetone, filtration to remove sparingly soluble $^tBu_3SiC{\equiv}CSi^tBu_3$, and subsequent sublimation yielded $HC{\equiv}CSi^tBu_3$ in 69% yield as a colorless, waxy solid. Its ^1H NMR (C_6D_6) spectrum displayed the expected ^{t}Bu and acetylenic resonances at δ 1.19 and 2.04, respectively, while the IR spectrum revealed C≡C and C−H stretches at 2032 and 3294 cm^{-1} (Table 1).

Deprotonation of $^tBu_3SiC{\equiv}CH$ by ^{n}BuLi in Et_2O produced $LiC{\equiv}CSi^tBu_3(OEt_2)_x$ in 73% yield upon crystallization from ether (eq 2). Although the Li reagent was used in the procedures below, the potassium analogue was also prepared. Deprotonation of $^tBu_3SiC{\equiv}CH$ with KH in THF occurred over 12 h at 22 °C, affording colorless $KC{\equiv}CSi^tBu_3$ (71%, eq 3), which was crystallized from ether.

$$^tBu_3SiC{\equiv}CH + {}^nBuLi \xrightarrow[25\ ^\circ C,\ 30\ min]{Et_2O,\ -BuH} {}^tBu_3SiC{\equiv}CLi(OEt_2)_x \quad (x \sim 0.2) \quad (2)$$

$$^tBu_3SiC{\equiv}CH + KH \xrightarrow[22\ ^\circ C,\ 12\ h]{THF,\ -H_2} KC{\equiv}CSi^tBu_3 \quad (3)$$

$\{L_xLi(^tBu_3SiC{\equiv}C)_2\}M(C{\equiv}CSi^tBu_3)_3L$ (M = Zr, Hf). (1) Syntheses. The original reactions of $ZrCl_4$ and $HfCl_4$ with $LiC{\equiv}CSi^tBu_3$ were aimed at stoichiometric substitution of the chlorides. $ZrCl_4$ was treated with 4 or 5 equiv of $LiC{\equiv}CSi^tBu_3$ in THF, and the product was recrystallized from ether. The resulting colorless microcrystals had a ^1H NMR spectrum that indicated a 5:3 ratio of $C{\equiv}CSi^tBu_3$ to THF. Elemental analysis revealed one lithium atom per molecule, implying the formula $LiZr(C{\equiv}CSi^tBu_3)_5(THF)_3$ (**1**, eq 4). ^1H (−80 to +23 °C) and

$$ZrCl_4 + 5LiC{\equiv}CSi^tBu_3 \xrightarrow[22\ ^\circ C,\ 12\ h]{THF,\ -4LiCl} \underset{\mathbf{1}}{\{(THF)_2Li(^tBu_3SiC{\equiv}C)_2\}Zr(C{\equiv}CSi^tBu_3)_3(THF)} \quad (4)$$

$$HfCl_4 + 5LiC{\equiv}CSi^tBu_3 \xrightarrow[22\ ^\circ C,\ 12\ h]{Et_2O,\ -4LiCl} \underset{\mathbf{2}}{\{(Et_2O)Li(^tBu_3SiC{\equiv}C)_2\}Hf(C{\equiv}CSi^tBu_3)_3(OEt_2)} \quad (5)$$

$^{13}C\{^1H\}$ NMR spectra, and IR (ν(C≡C) = 2015 cm^{-1}, Nujol mull) spectra failed to distinguish different $C{\equiv}CSi^tBu_3$ ligands (Table 1). Treatment of $HfCl_4$ with 5 equiv of $LiC{\equiv}CSi^tBu_3$ in Et_2O afforded a colorless, crystalline material whose ^1H and $^{13}C\{^1H\}$ NMR spectra implicated the formula $LiHf(C{\equiv}CSi^tBu_3)_5(OEt_2)_2$ (**2**, eq 5). Aside from the difference in the number of ether units, the complex appeared related to **1**, manifesting a single IR band at 2022 cm^{-1} that was attributed to the acetylides.

(2) X-ray Structural Study of 1. The single-crystal X-ray structural study (Table 2) of $\{(THF)_2Li(^tBu_3SiC{\equiv}C)_2\}Zr(C{\equiv}CSi^tBu_3)_3(THF)$ (**1**) resulted in the molecular structure shown in Figure 1a. The distorted octahedron of five alkynyls and one THF ligand (d(Zr−O1) = 2.285(4) Å) can be roughly rationalized on the basis of greater interligand repulsion between different $C{\equiv}CSi^tBu_3$ ligands ($\angle CZrC_{av}$ = 92.4(44)°) versus THF/$C{\equiv}CSi^tBu_3$ interactions ($\angle CZrO(THF)_{av}$ = 84.8(28)°, Table 3).

The lithium resides between two of the alkynyls and is coordinated by two THF molecules, giving it a distorted

(12) Wolczanski, P. T.; Bercaw, J. E. *Organometallics* **1982**, *1*, 793−799.

(13) For a review containing early $Cp_2M(C_2R)_2$ (M = Ti, Zr, Hf) chemistry and the author's pioneering studies of homoleptic late metal acetylides, see: Nast, R. *Coord. Chem. Rev.* **1982**, *47*, 89−124.

(14) Manna, J.; John, K. D.; Hopkins, M. D. *Adv. Organomet. Chem.* **1995**, *38*, 79−154.

(15) Kawaguchi, H.; Tatsumi, K. *Organometallics* **1995**, *14*, 4294−4299, and references cited therein.

(16) For related lanthanide complexes, $LiLn(C{\equiv}CR)_4(THF)$ (Ln = lanthanide), see: Evans, W. J.; Wayda, A. L. *J. Organomet. Chem.* **1980**, *202*, C6−C8.

(17) John, K. D.; Geib, S. J.; Hopkins, M. D. *Organometallics* **1996**, *15*, 4357−4361.

(18) (a) Cuenca, T.; Gómez, R.; Gómez-Sal, P.; Rodriguez, G. M.; Royo, P. *Organometallics* **1992**, *11*, 1229−1234. (b) Sekutowski, D. G.; Stucky, G. D. *J. Am. Chem. Soc.* **1989**, *111*, 1376−1382. (c) Wood, G. L.; Knobler, C. B.; Hawthorne, M. F. *Inorg. Chem.* **1989**, *28*, 382−384. (d) Erker, G.; Frömberg, W.; Benn, R.; Mynott, R.; Angermund, K.; Krüger, C. *Organometallics* **1989**, *8*, 911−920.

(19) (a) Heeres, H. J.; Nijhoff, J.; Teuben, J. H.; Rogers, R. D. *Organometallics* **1993**, *12*, 2609−2617. (b) Examples of the microscopic reverse (dinuclear oxidative addition of diacetylenes): Rosenthal, U.; Ohff, A.; Baumann, W.; Kempe, R.; Tillack, A.; Burlakov, V. V. *Organometallics* **1994**, *13*, 2903−2906. Rosenthal, U.; Ohff, A.; Tillack, A.; Baumann, W.; Görls, H. *J. Organomet. Chem.* **1994**, *468*, C4−C8.

(20) A recent theoretical study: Jemmis, E. D.; Giju, K. T. *Angew. Chem., Int. Ed. Engl.* **1997**, *36*, 606−608.

(21) (a) Neithamer, D. R.; LaPointe, R. E.; Wheeler, R. A.; Richeson, D. S.; Van Duyne, G. D.; Wolczanski, P. T. *J. Am. Chem. Soc.* **1989**, *111*, 9056−9072. (b) Bonanno, J. B.; Henry, T. P.; Neithamer, D. R.; Wolczanski, P. T.; Lobkovsky, E. B. *J. Am. Chem. Soc.* **1996**, *118*, 5132−5133.

(22) (a) Covert, K. J.; Wolczanski, P. T.; Hill, S. A.; Krusic, P. J. *Inorg. Chem.* **1992**, *31*, 66−78. (b) Covert, K. J.; Neithamer, D. R.; Zonnevylle, M. C.; LaPointe, R. E.; Schaller, C. P.; Wolczanski, P. T. *Inorg. Chem.* **1991**, *30*, 2494−2508.

(23) Eppley, D. F.; Wolczanski, P. T.; Van Duyne, G. D. *Angew. Chem., Int. Ed. Engl.* **1991**, *30*, 584−585.

(24) Wolczanski, P. T. *Polyhedron* **1995**, *22*, 3335−3362.

(25) Nowakowski, P. M.; Sommer, L. H. *J. Organomet. Chem.* **1979**, *179*, 95−103.

Table 1. ^{1}H and ^{13}C{^{1}H} NMR[a] and Selected Infrared Spectral Data[b] for (^{t}Bu$_3$SiC≡C)$_n$M Derivatives

	^{1}H NMR (δ, assgmt, mult, J (Hz))		^{13}C{^{1}H} NMR (δ, assgmt, J (Hz))			
compound	((H$_3$C)$_3$C)$_3$	other	C(*C*H$_3$)$_3$	*C*(CH$_3$)$_3$	other	(ν(C≡C), cm^{-1})
^{t}Bu$_3$SiC≡CH	1.19	2.04 (H)	30.83	21.99	87.09 (SiC≡) 96.47 (≡CH)	2032 3294 (ν(CH))
^{t}Bu$_3$SiC≡CSi^{t}Bu$_3$	1.24		31.00	22.30	114.16 (C≡C)	
^{t}Bu$_3$SiC≡CLi[c]	1.31		31.41	22.37	110.97 (SiC≡) 170.61 (≡CLi)	1987
^{t}Bu$_3$SiC≡CK[c]	1.28		31.55	22.20	111.56 (SiC≡) 187.57 (≡CK)	
{(THF)$_2$Li(^{t}Bu$_3$SiC≡C)$_2$}Zr (C≡CSi^{t}Bu$_3$)$_3$(THF) (**1**)[d]	1.33	1.56 (CH$_2$, m) 4.09 (CH$_2$O, m)	31.56	22.40	26.05 (CH$_2$) 71.39 (CH$_2$O) 106.64 (SiC≡) 173.79[e](≡CZr)	2015
{(Et$_2$O)Li(^{t}Bu$_3$SiC≡C)$_2$}Hf (C≡CSi^{t}Bu$_3$)$_3$(OEt$_2$) (**2**)	1.32	1.22 (CH$_3$, m) 3.90 (CH$_2$O, m)	31.46	22.36	15.08 (CH$_3$) 68.00 (CH$_2$O) 111.26 (SiC≡) 166.88(≡CZr)	2022
{Li(^{t}Bu$_3$SiC≡C)$_3$}Ta(C≡CSi^{t}Bu$_3$)$_3$ (**3**)[d]	1.33		31.71	22.60	127.73 (SiC≡) 199.20(≡CTa)	2015
3[c]			32.03	22.84	120.76 (SiC≡) 208.23(≡CTa)	
[K(crypt 2.2.2)][Ta(C≡CSi^{t}Bu$_3$)$_6$] (**5**)[f]	1.18	2.58 (NCH$_2$, t) 3.54−3.69 (OCH$_2$, m)	32.03	22.84	54.90 (NCH$_2$) 68.53 (OCH$_2$) 71.36 (OCH$_2$) 120.76 (SiC≡) 208.23(≡CTa)	2012
{Li(^{t}Bu$_3$SiC≡C)$_3$}$_2$Zr (**6**)	1.31		31.49	22.38	114.35 (SiC≡) 171.20 (≡CZr)	2016
{Li(^{t}Bu$_3$SiC≡C)$_3$}$_2$Hf (**7**)	1.31		31.47	22.32	115.18 (SiC≡) 175.82 (≡CZr)	2028

[a] C$_6$D$_6$ solvent. [b] Nujol mull. [c] ^{13}C{^{1}H} NMR spectra in THF-d_8. [d] ^{1}H NMR spectra (−80 to +23 °C) showed only one ^{t}Bu$_3$Si resonance. [e] Signal observation tentative. [f] Crypt 2.2.2 = N(CH$_2$CH$_2$OCH$_2$CH$_2$OCH$_2$CH$_2$)$_3$N.

tetrahedral coordination sphere. Interaction of the two alkynes with lithium is asymmetric, as evidenced by the C9−Li and C5−Li distances, 2.329(14) and 2.405(13) Å, respectively. The shorter C9−Li distance is accompanied by a long C9−Zr bond length, 2.386(6) Å, as compared to an average of 2.308 Å for the other zirconium−alkynyl bonds. In this coordination environment, the lithium−C5 and −C9 distances are shorter than the lithium−C6 and −C10 distances by 0.54 and 0.59 Å, respectively. The differences are similar to those in (C$_5$Me$_5$)$_2$Y(C≡C^{t}Bu)$_2$Li(THF) (0.53 Å)[26] and significantly larger than those in a Ti(III) compound with analogous lithium−alkynyl interactions, (Me$_4$HC$_5$)$_2$Ti{(C≡CC≡CSiMe$_3$)$_2$Li(THF)$_2$}, where the difference is 0.26 Å.[27] The larger variance in **1** is explained by the fact that the two ligating alkynes are significantly bent outward, with Zr−C−C angles of 162.0(5) and 166.1(5)°, due to steric interactions between the Si^{t}Bu$_3$ groups and the THF molecules bound to the lithium, as indicated by the space-filling view in Figure 1b. These contacts are also seen in the expansion of the O2−Li−O3 angle to 113.0(6)°, compared to an angle of 100.5° in (Me$_4$HC$_5$)$_2$Ti{(C≡CC≡CSiMe$_3$)$_2$Li(THF)$_2$}.[27]

The average zirconium−alkynyl bond length of 2.324 Å can be compared to three cyclopentadienyl zirconium alkynyls with an average zirconium−alkynyl bond length of 2.260 Å.[14] The metal−alkynyl bonds of **1** are 0.06 Å longer, perhaps reflecting the formal −1 charge on zirconium. Analogously, the average Zr−C bond distance of 2.38 Å in [Li(tmeda)]$_2$[ZrMe$_6$][5] is 0.10 Å longer than the zirconium−methyl distance in Cp$_2$ZrMe$_2$.[28] The strong σ donating ability of the alkynyls is manifested in their trans influence. Zr−C9 is the longest bond at 2.386(6) Å, presumably due to its interaction with lithium, and the two shortest bonds are Zr−C7 (2.293(6) Å) and Zr−C5 (2.274(7) Å), which are trans to C9 and the THF ligand, respectively. Finally, Zr−C1 and Zr−C3 are trans to each other and have intermediate bond lengths, 2.335(6) and 2.331(5) Å, respectively.

The C≡C bond lengths range from 1.210(7) to 1.247(8) Å, and while these distances are within error (3σ), they are strikingly long. The mean of all reported MC≡CR bond distances with an estimated standard deviation (esd) ≤ 0.010 Å is 1.201 Å, and none are longer than 1.230 Å.[14] Two of the three especially long bonds are coordinated to the Li$^+$,[29] and some elongation might be attributed to donation of electron density from their π-bonding orbitals to Li. However, given the only slightly longer than normal distances attributed to the acetylenic bonds in {(Et$_2$O)Li(^{t}Bu$_3$SiC≡C)$_2$}Hf(C≡CSi^{t}Bu$_3$)$_3$(OEt$_2$) (**2**, vide infra), and the greater error in cell parameters intrinsic to synchrotron data collection, the C≡C bond lengths in **1** are probably somewhat long but within the common range.[14] In the 12e$^-$ complex {(THF)$_2$Li(^{t}Bu$_3$SiC≡C)$_2$}Zr(C≡CSi^{t}Bu$_3$)$_3$(THF) (**1**), slightly long C≡C distances are best rationalized as a consequence of the intrinsic polarization (i.e., Zrδ^+−Cδ^-) pertaining to the zirconium−carbon bond.[14,30] Ab initio calculations on the anion [C≡CH]$^-$ suggest a C≡C distance of 1.2463(10) Å, which is ∼0.04 Å longer than the bond in acetylene because the lone pair of the alkynyl anion is slightly σ-antibonding in character; therefore, a partial negative charge on an sp carbon should also lengthen the C≡C bonds of the alkynyl ligands.

(26) Evans, W. J.; Drummond, D. K.; Hanusa, T. P.; Olofson, J. M. *J. Organomet. Chem.* **1989**, *376*, 311−320.
(27) Varga, V.; Mach, K.; Hiller, J.; Thewalt, U. *J. Organomet. Chem.* **1996**, *506*, 109−112.
(28) Hunter, W. E.; Hrncir, D. C.; Bynum, R. V.; Penttila, R. A.; Atwood, J. L. *Organometallics* **1983**, *2*, 750−755.
(29) For a discussion of lithium−alkyne π-interactions with leading references see: Goldfuss, B.; Schleyer, P. v. R.; Hampel, F. *J. Am. Chem. Soc.* **1997**, *119*, 1072−1080.
(30) For a recent computational assessment of early metal acetylide bonding, see: De Angelis, F.; Re, N.; Rosi, M.; Sgamellotti, A.; Floriani, C. *J. Chem. Soc., Dalton Trans.* **1997**, 3841−3844.

Table 2. X-ray Crystallographic Data on Alkynyl Derivatives (Crystal Data, Data Collection and Refinement)

	{(THF)$_2$Li(^{t}Bu$_3$SiC≡C)$_2$}-Zr(C≡CSi^{t}Bu$_3$)$_3$(THF) (**1**)	{(Et$_2$O)Li(^{t}Bu$_3$SiC≡C)$_2$}-Hf(C≡CSi^{t}Bu$_3$)$_3$(OEt$_2$) (**2**)	{Li(^{t}Bu$_3$SiC≡C)$_3$}-Ta(C≡CSi^{t}Bu$_3$)$_3$ (**3**)	[K(crypt 2.2.2)]-[Ta(C≡CSi^{t}Bu$_3$)$_6$] (**5**)	{Li(^{t}Bu$_3$SiC≡C)$_3$}$_2$Zr (**6**)	{Li(^{t}Bu$_3$SiC≡C)$_3$}$_2$Hf (**7**)
formula	$C_{88}H_{174}LiO_{4.5}Si_5Zr$	$C_{78}H_{155}LiO_2Si_5Hf$	$C_{84}H_{162}LiSi_6Ta$	$C_{105}H_{201}KN_2O_6Si_6Ta$	$C_{84}H_{162}Li_2Si_6Zr$	$C_{84}H_{162}Li_2Si_6Hf$
fw	1566.90	1450.90	1528.57	1976.21	1445.78	1533.05
cryst system	triclinic	monoclinic	trigonal (hex)	triclinic	rhombohedral (hex)	rhombohedral (hex)
space group	$P\bar{1}$	Cc	$R\bar{3}c$	$P\bar{1}$	$R\bar{3}$	$R\bar{3}$
Z	2	4	6	2	3	3
a, Å	15.490(3)	15.6682(3)	22.056(4)	15.1113(2)	14.73210(10)	14.719(2)
b, Å	16.319(3)	47.7280(1)	22.056(4)	17.7254(1)	14.73210(10)	14.719(2)
c, Å	22.886(5)	13.7380(2)	37.398(7)	22.6003(5)	38.6313(2)	39.206(8)
α, deg	69.55(3)	90.000(1)	90	86.312(1)	90	90
β, deg	82.66(3)	117.5788(8)	90	86.788(1)	90	90
γ, deg	70.14(3)	90.000(1)	120	86.760(1)	120	120
V, Å^3	5098(2)	9106.1(2)	15756(5)	6023.1(2)	7261.04(8)	7356(2)
D (calc), g·cm^{-3}	1.022	1.058	0.967	1.090	0.992	1.038
abs coeff, mm^{-1}	0.209	1.248	1.147	1.058	0.223	1.172
F(000)	1726	3136	4956	2138	2388	2484
cryst size, mm	0.4 × 0.2 × 0.2	0.3 × 0.2 × 0.15	0.3 × 0.6 × 0.7, 0.4 × 0.5 × 0.6	0.40 × 0.40 × 0.35	0.4 × 0.3 × 0.3	0.3 × 0.2 × 0.2
temp, K	293	293	293	223(2)	173	293
radiation λ, Å	0.914 (synchrotron)	0.710 73 (Mo Kα)	0.710 73 (Mo Kα)	0.710 73 (Mo Kα)	0.710 73 (Mo Kα)	0.710 73 (Mo Kα)
θ limits, deg	2.99−27.06	1.53−28.41	1.85−22.51	1.15−28.23	1.58−28.20	1.56−23.29
limiting indicies	$0 \le h \le +15$, $-15 \le k \le +16$, $-22 \le l \le +22$	$-19 \le h \le +19$, $-62 \le k \le +33$, $-16 \le l \le +17$	$0 \le h \le 22$, $-23 \le k \le 0$, $-8 \le l \le 40$	$-19 \le h \le 19$, $-23 \le k \le 23$, $0 \le l \le 30$	$-18 \le h \le +17$, $-18 \le k \le +10$, $-50 \le l \le +49$	$-16 \le h \le +11$, $-14 \le k \le +16$, $-43 \le l \le +43$
reflecns collected	7969	27404	4453	28856	8233	10464
independent refecns	7969	17044	2295 (R_{int} = 0.0427)	25821 (R_{int} = 0.0523)	3699 (R_{int} = 0.0379)	2366 (R_{int} = 0.1366)
refinement method	full-matrix, least-squares on F^2	full-matrix, least-squares on F^2	full-matrix, least-squares on F^2	full-matrix, least-squares on F^2	full-matrix, least-squares on F^2	full-matrix, least-squares on F^2
data/restraints/param	7966/0/899	11643/2/784	2292/0/141	25806/0/1075	3697/0/143	1300/0/140
GOF on F^2	0.965	1.020	1.005	0.970	1.932	1.068
R indicies [$I > 2\sigma(I)$]	R_1 = 0.0747, R_{w2} = 0.2079	R_1 = 0.0426, R_{w2} = 0.0816	R_1 = 0.0500, wR_2 = 0.1334	R_1 = 0.0465, R_{w2} = 0.1183	R_1 = 0.0519, R_{w2} = 0.1548	R_1 = 0.0625, R_{w2} = 0.1449
R indicies (all data)	R_1 = 0.0765, R_{w2} = 0.2134	R_1 = 0.0834, R_{w2} = 0.1141	R_1 = 0.0752, R_{w2} = 0.1549	R_1 = 0.0659, R_{w2} = 0.1409	R_1 = 0.0592, R_{w2} = 0.1645	R_1 = 0.1158, R_{w2} = 0.1871
largest diff peak/hole, e·Å^{-3}	+0.523 and −0.443	+0.424 and −0.367	+0.882 and −1.092	+1.683 and −2.064	+0.762 and −0.517	+0.811 and −0.381

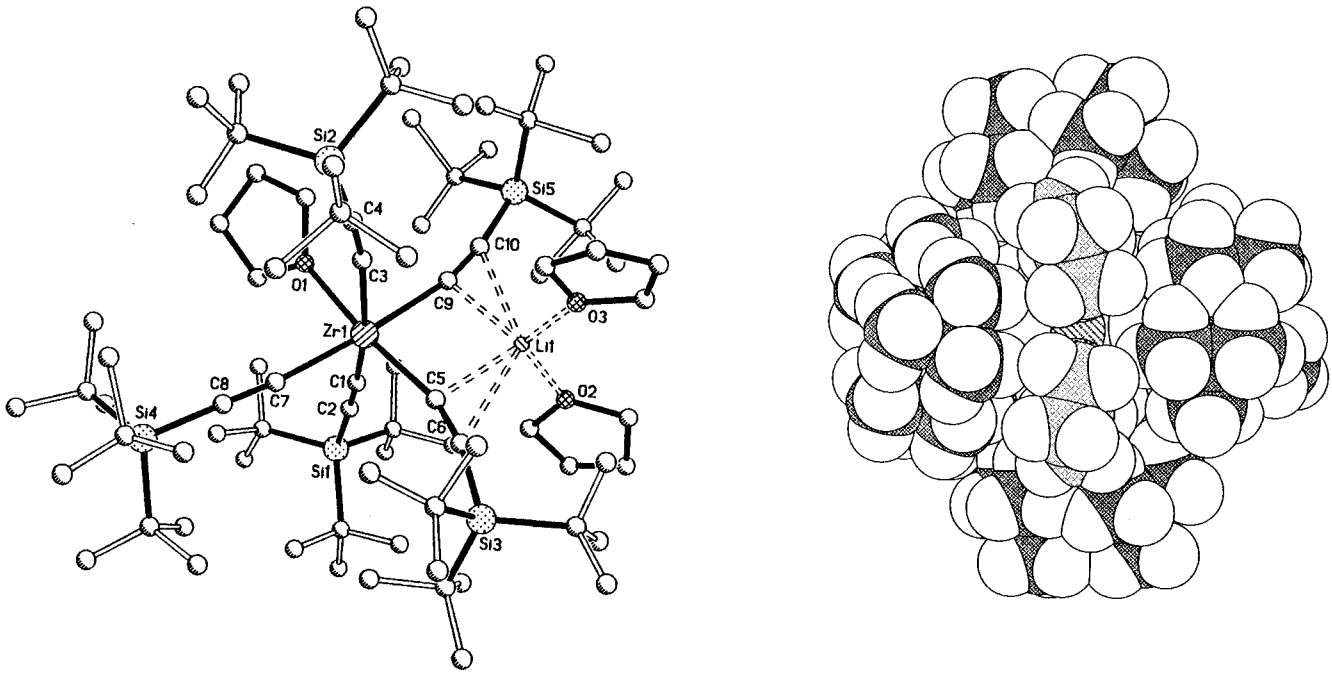

Figure 1. Molecular (a) and space-filling (b, note THF/C≡CSi^{t}Bu$_3$ interactions) views of {(THF)$_2$Li(^{t}Bu$_3$SiC≡C)$_2$}Zr(C≡CSi^{t}Bu$_3$)$_3$(THF) (**1**).

Table 3. Selected Bond Lengths (Å) and Angles (deg) for {(THF)$_2$Li(^{t}Bu$_3$SiC≡C)$_2$}Zr(C≡CSi^{t}Bu$_3$)$_3$(THF) (**1**)

Zr−C1	2.335(6)	C1−C2	1.230(8)	C2−Si1	1.862(6)
Zr−C3	2.331(5)	C3−C4	1.210(7)	C4−Si2	1.874(5)
Zr−C5	2.274(7)	C5−C6	1.247(8)	C6−Si3	1.878(7)
Zr−C7	2.293(6)	C7−C8	1.244(8)	C8−Si4	1.859(6)
Zr−C9	2.386(6)	C9−C10	1.245(7)	C10−Si5	1.877(5)
Zr−O1	2.285(4)	Li−C5	2.405(13)	Li−C9	2.329(14)
Li−O2	1.944(10)	Li−C6	2.996(15)	Li−C10	2.871(15)
Li−O3	1.943(13)				
C1−Zr−C3	165.2(2)	C7−Zr−C9	173.1(2)	Zr−C7−C8	174.2(5)
C1−Zr−C5	98.7(2)	C1−Zr−O1	84.2(2)	Zr−C9−C10	166.1(5)
C1−Zr−C7	90.3(2)	C3−Zr−O1	81.3(2)	C1−C2−Si1	176.1(5)
C1−Zr−C9	85.7(2)	C5−Zr−O1	173.9(2)	C3−C4−Si2	174.9(5)
C3−Zr−C5	95.4(2)	C7−Zr−O1	87.9(2)	C5−C6−Si3	168.0(6)
C3−Zr−C7	92.5(2)	C9−Zr−O1	85.7(2)	C7−C8−Si4	178.5(6)
C3−Zr−C9	89.2(2)	Zr−C1−C2	175.9(5)	C9−C10−Si5	170.9(5)
C5−Zr−C7	97.3(2)	Zr−C3−C4	172.0(5)	O2−Li−O3	113.0(6)
C5−Zr−C9	89.2(2)	Zr−C5−C6	162.0(5)		

(3) X-ray Structural Study of 2. The single-crystal X-ray structural study (Table 2) of {(Et$_2$O)Li(^{t}Bu$_3$SiC≡C)$_2$}Hf(C≡CSi^{t}Bu$_3$)$_3$(OEt$_2$) (**2**) revealed a distorted octahedral structure containing five alkynyls—two bridged by Li(OEt$_2$)—and one ether (Figure 2). One of the alkynyls bound to Li has a long hafnium−carbon distance (d(Hf−C7) = 2.387(7) Å), and the alkynyl trans to it is slightly shorter (d(Hf−C3) = 2.263(8) Å) (Table 4). Hafnium−carbon bonds of the remaining C≡CSi^{t}Bu$_3$ ligands average 2.292(10) Å in length, including the other bound to Li, which is opposite the ether, a ligand with a smaller trans influence than an alkynyl. The hafnium−ether bond length is 2.270(5) Å, and it is likely that neither the ether nor the THF in {(THF)$_2$Li(^{t}Bu$_3$SiC≡C)$_2$}Zr(C≡CSi^{t}Bu$_3$)$_3$(THF) (**1**) are significant π-donors. Compared to Et$_2$O∠C≡CSi^{t}Bu$_3$ interactions (∠CHfO1$_{av}$ = 87.0(16)°, interligand repulsions between different C≡CSi^{t}Bu$_3$ ligands are greater (∠CHfC$_{av}$ = 93.9(21)°), except for ∠C5HfC7 = 82.8(2)° and ∠C1ZrC7= 85.2(2)°, which reflect the longer bond length of the C7-containing alkynyl.

Although ∠C7HfC9 = 90.1(3)°, the Li-bound alkynyls are again splayed away from the Li(OEt) group, with ∠HfC7C8 = 165.6(6)° and ∠HfC9C10 = 161.6(6)° compared to ∠HfCC$_{av}$ = 173.4(6)° for the remaining alkynyls. The lithium is symmetrically bound in the Hf derivative, with d(C7−Li) = 2.21(2), d(C8−Li) = 2.82(2), d(C9−Li) = 2.23(2), and d(C10−Li) = 2.89(2) Å. The alkynyl triple bond lengths are normal (d(C≡C)$_{av}$ = 1.203(16) Å) and the Li-bound and simple η^1-alkynyls are alike. In general, structural features of **2** parallel those of **1**, and the above discussion is applicable.[14]

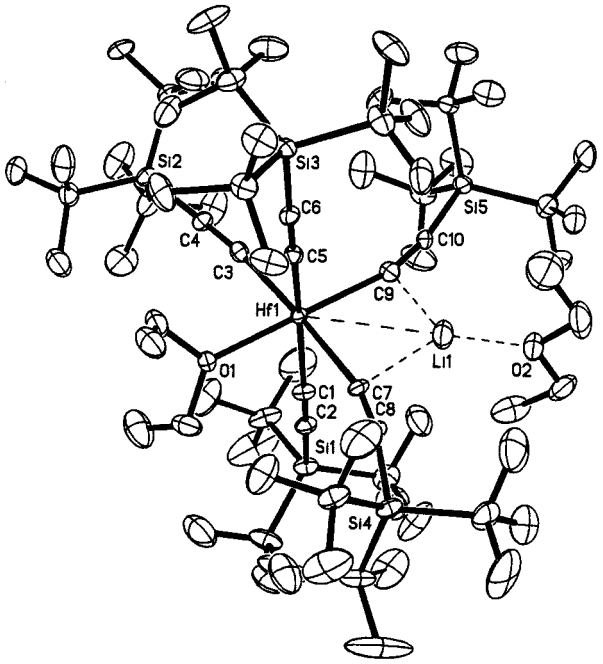

Figure 2. Molecular view of {(Et$_2$O)Li(^{t}Bu$_3$SiC≡C)$_2$}Hf(C≡CSi^{t}Bu$_3$)$_3$(OEt$_2$) (**2**).

{Li(^{t}Bu$_3$SiC≡C)$_3$}Ta(C≡CSi^{t}Bu$_3$)$_3$ (3). (1) Synthesis. Treatment of TaCl$_5$ with 6 equiv of LiC≡CSi^{t}Bu$_3$ in benzene provided {Li(^{t}Bu$_3$SiC≡C)$_3$}Ta(C≡CSi^{t}Bu$_3$)$_3$ (**3**), which was isolated as yellow, light-sensitive microcrystals from ether in 68% yield (eq 6). Again, ^{1}H (−80 to +23 °C) and ^{13}C NMR spectra and the IR (ν(C≡C) = 2015 cm^{-1}) spectrum of **3** were all consistent with only one environment for the C≡CSi^{t}Bu$_3$

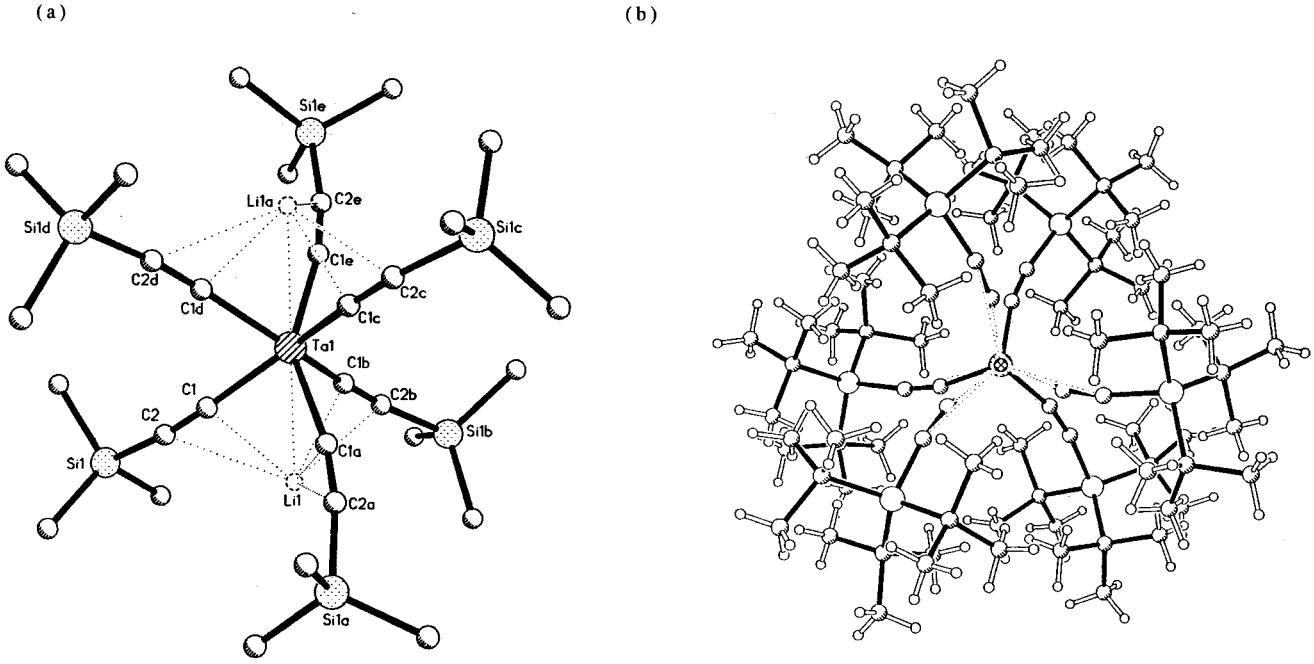

Figure 3. Molecular views of $\{Li(^tBu_3SiC{\equiv}C)_3\}Ta(C{\equiv}CSi^tBu_3)_3$ (**3**) showing the 2-fold Li disorder (a, Me groups removed for clarity) and the twisted prism geometry (b, 18° twist down the LiTa axis).

Table 4. Selected Bond Lengths (Å) and Angles (deg) for $\{(Et_2O)Li(^tBu_3SiC{\equiv}C)_2\}Hf(C{\equiv}CSi^tBu_3)_3(OEt_2)$ (**2**)

Hf−C1	2.292(8)	C1−C2	1.192(10)	C2−Si1	1.848(8)
Hf−C3	2.263(8)	C3−C4	1.218(9)	C4−Si2	1.849(8)
Hf−C5	2.302(7)	C5−C6	1.211(9)	C6−Si3	1.837(7)
Hf−C7	2.387(7)	C7−C8	1.181(9)	C8−Si4	1.876(8)
Hf−C9	2.282(8)	C9−C10	1.214(9)	C10−Si5	1.852(8)
Hf−O1	2.270(5)	Li−C7	2.21(2)	Li−C8	2.82(2)
Li−O2	1.91(2)	Li−C9	2.23(2)	Li−C10	2.89(2)
C1−Hf−C3	96.6(3)	C7−Hf−C9	90.1(3)	Hf−C7−C8	165.6(6)
C1−Hf−C5	86.0(2)	C1−Hf−O1	86.4(2)	Hf−C9−C10	161.6(6)
C1−Hf−C7	89.4(2)	C3−Hf−O1	86.3(2)	C1−C2−Si1	172.7(7)
C1−Hf−C9	179.5(3)	C5−Hf−O1	86.0(2)	C3−C4−Si2	177.6(7)
C3−Hf−C5	94.8(3)	C7−Hf−O1	89.4(2)	C5−C6−Si3	176.0(7)
C3−Hf−C7	175.3(3)	C9−Hf−O1	179.5(3)	C7−C8−Si4	169.4(7)
C3−Hf−C9	94.2(3)	Hf−C1−C2	173.5(7)	C9−C10−Si5	168.5(7)
C5−Hf−C7	82.8(2)	Hf−C3−C4	172.7(6)		
C5−Hf−C9	94.2(3)	Hf−C5−C6	173.9(6)		

ligands, but elemental analysis indicated the presence of one lithium per tantalum. The addition of 5 equiv of $LiC{\equiv}CSi^tBu_3$ to $TaCl_5$ only resulted in a diminished crop of **3**, and a route to $Ta(C{\equiv}CSi^tBu_3)_5$ was not found.

$$TaCl_5 + 6\ LiC{\equiv}CSi^tBu_3 \xrightarrow[25\ °C,\ 12\ h]{C_6H_6,\ -5LiCl} \{Li(^tBu_3SiC{\equiv}C)_3\}Ta(C{\equiv}CSi^tBu_3)_3 \quad (6)$$
3

(2) X-ray Structural Study. A single-crystal X-ray structural determination (Table 2) of $\{Li(^tBu_3SiC{\equiv}C)_3\}Ta(C{\equiv}CSi^tBu_3)_3$ (**3**) revealed the twisted trigonal prismatic structure illustrated in Figure 3. The lithium is disordered between the two trigonal faces (Figure 3a), hence the $C{\equiv}CSi^tBu_3$ ligands are an average of lithium-bound and -unbound alknyls. No obvious signs of alkynyl disorder, such as elongated thermal ellipsoids or doubled atoms, were observed, suggesting that the two faces have very similar geometry. While no comparable tantalum alkynyl derivatives exist, the metrical data for **2** (Table 5) appear reasonable. The six crystallographically equivalent Ta−C distances of 2.138(6) Å are short when compared to the average

Table 5. Selected Interactomic Distances (Å) and Angles (deg) for $\{Li(^tBu_3SiC{\equiv}C)_3\}Ta(C{\equiv}CSi^tBu_3)_3$ (**3**)

Ta−C1	2.138(6)	C1−Li	2.26(2)
C1−C2	1.210(10)	C2−Li	2.732(12)
C2−Si	1.857(8)	Ta−Li	2.85(3)
Ta−C1−C2	168.2(7)	C1−Ta−C1d	78.7(4)
C1−C2−Si	169.7(8)	Si1−Ta−Si1a	89.6
C1−Ta−C1a	85.4(3)	Si1−Ta−Si1d	83.9

zirconium− and hafnium−alkynyl bond lengths of 2.32(4) Å in **1** and 2.31(5) Å in **2**, even when accounting for the smaller covalent radius of tantalum (r_{cov}(Zr) = 1.45 Å; r_{cov}(Hf) = 1.44 Å; r_{cov}(Ta) = 1.34 Å).[31] In **3**, the acetylenic bond lengths (d(C≡C) = 1.210(10) Å) appear long but are within the error of the mean of reported MC≡CR distances, 1.201 Å.[14] As in **1** and **2**, the Cα−Li distances (2.26(2) Å) are shorter than the Cβ−Li interactions (2.732(12) Å), probably as a consequence of occupying a trigonal face, but such interpretations must be tempered by the disorder problems.

A significant bending of the ligands is revealed by the M−C≡C and C≡C−Si angles, 168.2(7) and 169.7(8)°, respectively. Although within range of comparable angles in other complexes, their deviation from 180° is among the largest.[14] Figure 3b illustrates the 18° dihedral twist along the 3-fold axis that is responsible for the D_{3h} to D_3 core distortion of **3**. The twist from trigonal prismatic geometry and the bending of the alkynyl ligands originates in steric interactions between the Si^tBu_3 groups on opposing trigonal faces and allows the silicon atoms to achieve a nearly octahedral geometry about the tantalum: ∠SiTaSi = 83.9 and 89.6°. Crude molecular mechanics calculations support this assessment, and symmetry constraints do not permit an additional electronic stabilization unless a descent from $D_3 \rightarrow C_3$ is incurred. In conclusion, trigonal prismatic coordination around tantalum is electronically most favorable,[2−4,9] and the additional twist derives from steric forces.

[K(crypt 2.2.2)][Ta(C≡CSi^{t}Bu$_3$)$_6$] (5). (1) Synthesis. In the solid-state structure of $\{Li(^tBu_3SiC{\equiv}C)_3\}Ta(C{\equiv}CSi^tBu_3)_3$

(31) Pauling, L. *The Nature of the Chemical Bond*, 3rd ed.; Cornell University Press: Ithaca, NY, 1960; pp 172−174.

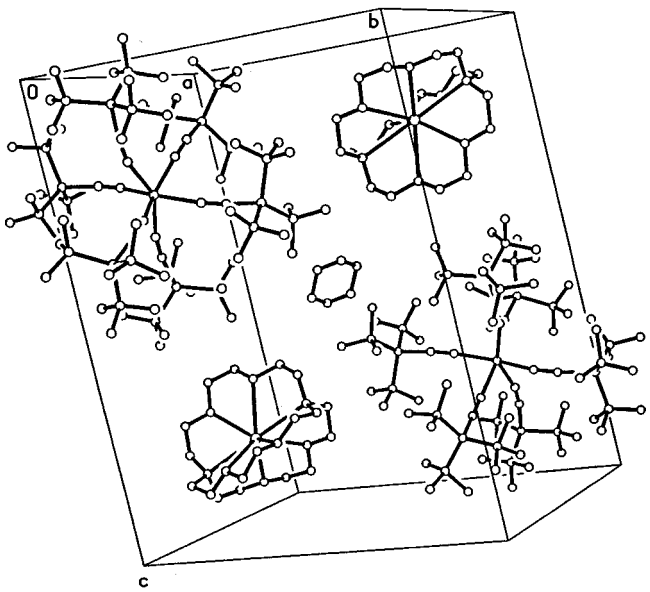

Figure 4. Unit cell of [K(crypt 2.2.2)][Ta(C≡CSi^{t}Bu$_3$)$_6$] (**5**), showing the ions and a benzene or disordered THF of crystallization.

(**3**), lithium occupies only one trigonal face of ligands, yet the two faces are crystallographically equivalent. Nevertheless, it is possible that the presence of the lithium cation perturbs the electronic environment of [Ta(C≡CSi^{t}Bu$_3$)$_6$]$^-$ enough to subtly alter its geometry. The addition of excess potassium triflate (5 equiv) to {Li(^{t}Bu$_3$SiC≡C)$_3$}Ta(C≡CSi^{t}Bu$_3$)$_3$ (**2**) in THF, followed by filtration in benzene, produced KTa(C≡CSi^{t}Bu$_3$)$_6$ (**4**, eq 7), which was not isolated. Treatment of **4** with excess crypt 2.2.2 in THF and crystal growth by hexane diffusion into a THF solution led to [K(crypt 2.2.2)][Ta(C≡CSi^{t}Bu$_3$)$_6$] (**5**) (eq 8). ^{13}C{^{1}H} NMR spectra of the [Ta(C≡CSi^{t}Bu$_3$)$_6$] unit in **5** taken in THF-d_8 were identical to **3**, implying a common [Ta(C≡CSi-^{t}Bu$_3$)$_6$]$^-$ anion.

$$\underset{\mathbf{3}}{\{\mathrm{Li}(^t\mathrm{Bu_3SiC{\equiv}C)_3\}Ta(C{\equiv}CSi^tBu_3)_3}} + \mathrm{KOTf} \xrightarrow[22\ ^\circ\mathrm{C},\ 12\ \mathrm{h}]{\mathrm{THF}} \underset{\mathbf{4}}{\mathrm{KTa(C{\equiv}CSi^tBu_3)_6}} + \mathrm{LiOTf} \quad (7)$$

$$\underset{\mathbf{4}}{\mathrm{KTa(C{\equiv}CSi^tBu_3)_6}} + \text{crypt 2.2.2} \xrightarrow[22\ ^\circ\mathrm{C},\ 12\ \mathrm{h}]{\mathrm{THF}} \underset{\mathbf{5}}{\mathrm{[K(crypt\ 2.2.2)][Ta(C{\equiv}CSi^tBu_3)_6]}} \quad (8)$$

(2) X-ray Structural Study. A single-crystal X-ray structural determination (Table 2) of [K(crypt 2.2.2)][Ta(C≡CSi^{t}Bu$_3$)$_6$] (**5**) revealed separate [K(crypt 2.2.2)]$^+$ and [Ta(C≡CSi-^{t}Bu$_3$)$_6$]$^-$ ions and either a benzene or disordered THF of crystallization for every two formula units (Figure 4). The bare [Ta(C≡CSi^{t}Bu$_3$)$_6$]$^-$ ion exhibits the twisted trigonal prismatic geometry shown in Figure 5, with a twist angle of ∼18° along the 3-fold axis, just as in {Li(^{t}Bu$_3$SiC≡C)$_3$}Ta(C≡CSi^{t}Bu$_3$)$_3$ (**3**). The C−Ta−C angles on the trigonal faces average 86.2-(11)°, while the corresponding angles bisecting the three 2-fold axes average 77.8(7)° (Table 6), values remarkably similar to those of **3** (85.4(3), 78.7(4)°). The tantalum−carbon bonds of **5** (d(TaC)$_{av}$ = 2.168(3) Å) are slightly lengthened relative to those of **3** (2.138(6) Å), and the alkyne bond lengths are within error of the lithium-bound derivative (d(C≡C)$_{av}$: **5**, 1.224(6); **3**, 1.210(10) Å). The Ta−C−C (**5**, 166.4(16) (av); **3**, 168.2-(7)°) and C−C−Si angles (**5**, 169.7(23) (av); **3**, 169.7(8)°) are also similar in accord with the related twist arising from aforementioned ^{t}Bu$_3$Si steric factors. It is clear that Li$^+$ coordination[29] in **3** has little, if any, effect on the coordination geometry of the [Ta(C≡CSi^{t}Bu$_3$)$_6$]$^-$ ion. By analogy, it is also doubtful that the tmeda-bound lithium cations in [ZrMe$_6$]Li$_2$-(tmeda)$_2$ have a pronounced influence on its trigonal prismatic structure.[5]

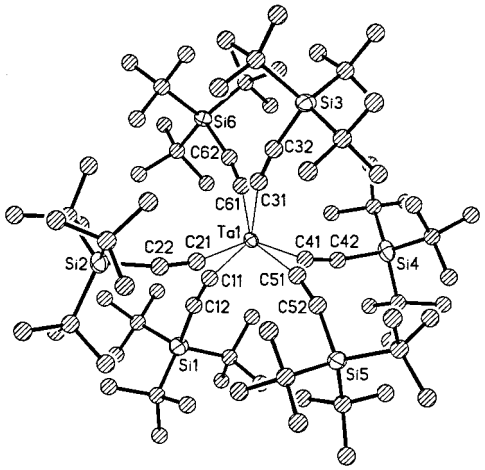

Figure 5. Anion of [K(crypt 2.2.2)][Ta(C≡CSi^{t}Bu$_3$)$_6$] (**5**) revealing the 18° twist down the C_3 axis.

{Li(^{t}Bu$_3$SiC≡C)$_3$}$_2$M (M = Zr, 6; Hf, 7). (1) Syntheses. Thermolyses of ZrCl$_4$ or HfCl$_4$ and 6 equiv of LiC≡CSi^{t}Bu$_3$ in benzene solution afforded colorless crystals of {Li(^{t}Bu$_3$SiC≡C)$_3$}$_2$M (M = Zr, **6** (17%); Hf, **7**, (38%)) upon slow evaporation of an ether solution. The moderate, unoptimized yields stem

$$\mathrm{MCl_4} + 6\mathrm{LiC{\equiv}CSi^tBu_3} \xrightarrow[4-12\ \mathrm{h}]{\mathrm{C_6H_6,\ 80\ ^\circ C}} \underset{\mathrm{M = Zr,\ \mathbf{6};\ Hf,\ \mathbf{7}}}{\{\mathrm{Li}(^t\mathrm{Bu_3SiC{\equiv}C)_3\}_2M}} \quad (9)$$

from difficulties in washing the hexaalkynyl species away from the salt cake with nonpolar, unreactive solvents. Both complexes displayed ^{1}H and ^{13}C{^{1}H} spectra indicative of a lone type of alkynyl and single ν(C≡C) IR bands at 2016 (**6**) and 2028 cm^{-1} (**7**).

(2) X-ray Structural Studies of 6 and 7. The single-crystal X-ray structural determinations (Table 2) of {Li(^{t}Bu$_3$SiC≡C)$_3$}$_2$M (M = Zr, **6**; Hf, **7**) revealed the near perfect octahedral structures illustrated in Figure 6 (Table 7) for this isomorphic pair. With three molecules in the unit cell, the rhombohedral (indexed hexagonal) space group (R3) requires an inversion center at the metal, hence a *trans*-alkynyl disposition of 180°. *cis*-C−Zr−C angles of 91.3(1) and 88.7(1)° define the remainder of the core of **6**, and the zirconium−carbon bond length of 2.263(3) Å is near the average of known cyclopentadienyl zirconium derivatives (2.260 Å).[13,14] Likewise, the *cis*-C−Hf−C angles of **7** are 90.2(3) and 89.8(4)°, with d(Hf−C) = 2.230(11) Å and d(C≡C) = 1.233(14) Å. The latter and the 1.218(4) Å C≡C bond length of the zirconium derivative are again longer than the average of known MC≡CR bond distances (1.201 Å) but not outside the reported range.[14] The lithium cations apparently reside in a hydrophobic pocket and are surrounded by the methyl groups of the ligands whose carbons are 2.9−3.6 Å away. While bare, uncoordinated lithium cations have not been previously crystallographically characterized, curiosity over this binding mode must be tempered by the knowledge that each Li$^+$ resides in a special position on the 3-fold axis and has a proportionately smaller electron density (1/3 Li$^+$ per asymmetric unit).

Table 6. Selected Bond Lengths (Å) and Angles (deg) for the $Ta(C{\equiv}CSi^tBu_3)_6^-$ Anion of $[K(crypt\ 2.2.2)][Ta(C{\equiv}CSi^tBu_3)_6]$ (**5**)

Ta−C11	2.168(4)		C11−C12	1.218(5)	
Ta−C21	2.169(4)		C21−C22	1.232(6)	
Ta−C31	2.165(4)		C31−C32	1.228(5)	
Ta−C41	2.163(4)		C41−C42	1.217(6)	
Ta−C51	2.168(4)		C51−C52	1.229(6)	
Ta−C61	2.173(4)		C61−C62	1.222(6)	
C11−Ta−C41	87.0(2)	Ta−C11−C12	166.1(4)	C11−C12−Si1	171.8(4)
C11−Ta−C61	87.7(2)	Ta−C21−C22	167.4(4)	C21−C22−Si2	168.3(4)
C41−Ta−C61	86.7(2)	Ta−C31−C32	165.7(4)	C31−C32−Si3	171.8(4)
C21−Ta−C31	85.4(2)	Ta−C41−C42	165.2(3)	C41−C42−Si4	169.3(4)
C21−Ta−C51	85.0(2)	Ta−C51−C52	164.7(3)	C51−C52−Si5	166.1(4)
C31−Ta−C51	85.4(2)	Ta−C61−C62	169.4(4)	C61−C62−Si6	170.9(4)
C11−Ta−C21	78.4(2)				
C31−Ta−C61	77.9(2)				
C41−Ta−C51	77.1(2)				

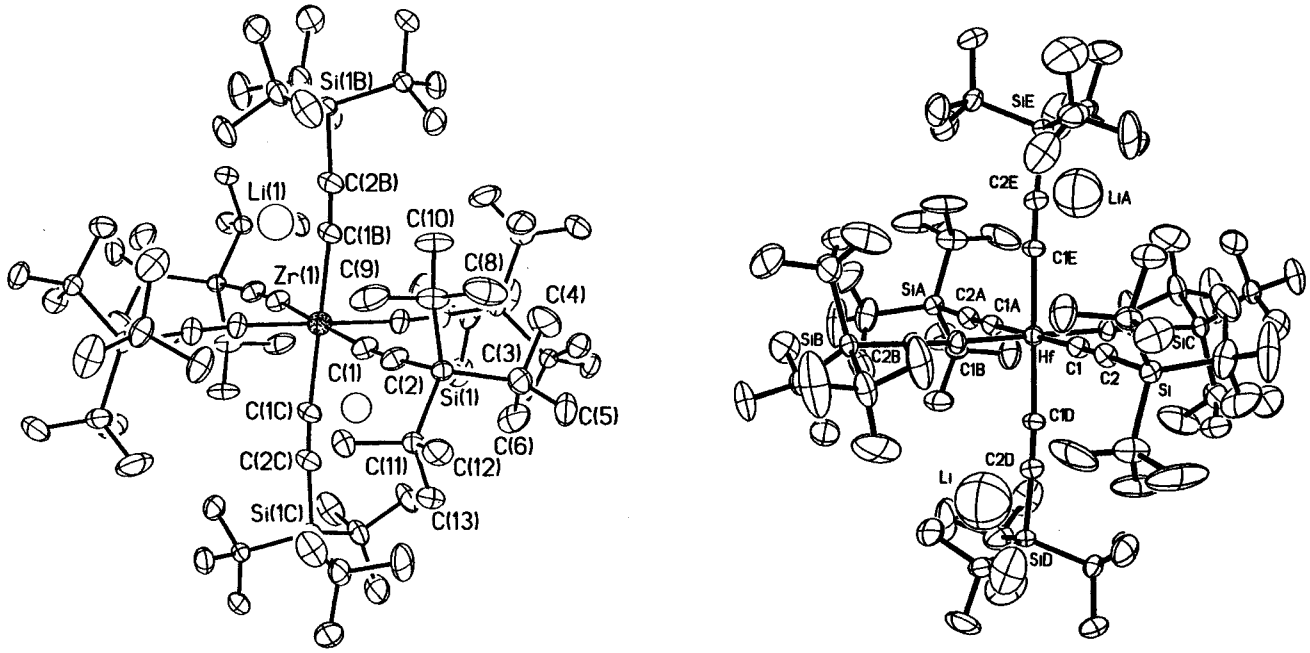

Figure 6. Molecular views of $\{Li(^tBu_3SiC{\equiv}C)_3\}_2Zr$ (**6**, left) and $\{Li(^tBu_3SiC{\equiv}C)_3\}_2Hf$ (**7**, right) octahedra. The Li atoms are buried in the hydrocarbon periphery (see text).

Table 7. Selected Bond Lengths (Å) and Angles (deg) for $\{Li(^tBu_3SiC{\equiv}C)_3\}_2Zr$ (**6**) and $\{Li(^tBu_3SiC{\equiv}C)_3\}_2Hf$ (**7**)

	Compound **6**		
Zr−C1	2.263(3)	Zr−C1−C2	174.3(3)
C1−C2	1.218(4)	C1−C2−Si	175.9(3)
C2−Si	1.849(3)	C1−Zr−C1a,c	91.29(10)
		C1−Zr−C1b,d	88.71(10)
	Compound **7**		
Hf−C1	2.230(11)	Hf−C1−C2	176.8(10)
C1−C2	1.233(14)	C1−C2−Si	177.2(10)
C2−Si	1.842(14)	C1−Hf−C1a,c	90.2(3)
		C1−Hf−C1b,d	89.8(4)

Discussion

Historical Perspective. Historically, the structural preference of d^0 early metal complexes was relevant to tris-bidentate complexes such as Cowie and Bennett's $M(S_2C_6H_4)_3^{n-}$ (M = Zr, $n = 2$;[32] Nb, $n = 1$,[33] Mo, $n = 0$),[34] where the ligand bite angle[35] and electronic factors related to the bidentate ligand proved critical. Only the recent synthesis and characterization of Girolami's $[ZrMe_6]Li_2(tmeda)_2$ [5] and Wilkinson's WMe_6 [6−8] provided examples of six-coordinate complexes comprised of monodentate ligands devoid of π-bonding capability. Both compounds are crucial examples of approximate trigonal prismatic geometry that support the theoretical contentions of Kang, Albright, Eisenstein,[2−4] and Kaupp,[9] i.e., that mixing of ligand-localized, filled σ-orbitals (HOMO) with empty, π-type orbitals (LUMO) in a d^0 system can result in stabilization of a trigonal prismatic structure relative to the VSEPR-predicted octahedron. Acetylide ligands also meet the "pure σ-donor" [30] requirements of ligands predicted to favor a trigonal prism, yet both geometries are observed.

Structural Dichotomy: D_3 $(^tBu_3SiC{\equiv}C)_6Ta^-$ vs O_h $(^tBu_3SiC{\equiv}C)_6M^{2-}$ (M = Zr, Hf). (1) Electroneutrality and VSEPR. Although questions regarding the structural influence of bound Li^+ have been answered via the virtually identical trigonal prisms accorded $\{Li(^tBu_3SiC{\equiv}C)_3\}Ta(C{\equiv}CSi^tBu_3)_3$ (**2**) and $[K(crypt\ 2.2.2)][Ta(C{\equiv}CSi^tBu_3)_6]$ (**3**), a structural dichotomy has arisen when octahedral $\{Li(^tBu_3SiC{\equiv}C)_3\}_2M$ (M = Zr, **6**; Hf, **7**) are considered. What is the origin of the structural difference between these seemingly homologous complexes?

(32) Cowie, M.; Bennett, M. J. *Inorg. Chem.* **1976**, *15*, 1595−1603.
(33) Cowie, M.; Bennett, M. J. *Inorg. Chem.* **1976**, *15*, 1589−11594.
(34) Cowie, M.; Bennett, M. J. *Inorg. Chem.* **1976**, *15*, 1584−1588.
(35) Larsen, E.; LaMar, G. N.; Wagner, B. E.; Parks, J. E.; Holm, R. H. *Inorg. Chem.* **1972**, *11*, 2652−2668.

Table 8. Structural Parameters Obtained via ADF (Prime) and GAMESS (Double Prime) Geometry Optimizations of $Ta(C{\equiv}CH)_6^-$ (**5′**, **5″**) and $Zr(C{\equiv}CH)_6^{2-}$ (**6′**, **6″**) Compared with Experimental Values for $Ta(C{\equiv}CSi^tBu_3)_6^-$, the Anion of [K(crypt 2.2.2)][$Ta(C{\equiv}CSi^tBu_3)_6$] (**5**), and $\{Li(^tBu_3SiC{\equiv}C)_3\}_2Zr$ (**6**)

		structural parameters[a]					
	geometry	M−C_α (Å)	C_α−C_β (Å)	∠M−C_α−C_β (deg)	C_3 twist (deg)	∠ϕ (deg)	∠δ (deg)
$Ta(C{\equiv}CSi^tBu_3)_6^-$ (**5**)[b]	D_3 (expt)	2.168(3)	1.224(6)	166.4(17)	18(1)	86.2(11)	77.8(7)
$Ta(C{\equiv}CH)_6^-$ (**5′**)	D_3	2.23	1.23	175.4	5.2	84.1	78.8
$Ta(C{\equiv}CH)_6^-$ (**5′**)	O_h[c]	2.27	1.24	180.0	60.0	90.0	90.0
$Ta(C{\equiv}CH)_6^-$ (**5″**)	D_{3h}[d]	2.19	1.23	179	0.0	84	79
$Ta(C{\equiv}CH)_6^-$ (**5″**)	O_h[e]	2.21	1.23	180.0	60.0	90.0	90.0
$\{Li(^tBu_3SiC{\equiv}C)_3\}_2Zr$ (**6**)	O_h (expt)	2.263(3)	1.218(4)	174.3(3)	60.0(10)	91.3(1)	88.7(1)
$Zr(C{\equiv}CH)_6^{2-}$ (**6′**)	D_3	2.36	1.24	178.4	0.0	84.6	78.0
$Zr(C{\equiv}CH)_6^{2-}$ (**6′**)	O_h[c]	2.39	1.24	180.0	60.0	90.0	90.0
$Zr(C{\equiv}CH)_6^{2-}$ (**6″**)	D_{3h}[f]	2.36	1.24	180	0.0	84.0	78.0
$Zr(C{\equiv}CH)_6^{2-}$ (**6″**)	O_h[g]	2.37	1.24	180	60	90	90

[a] Defined in Figure 7. [b] Average values; see Table 5 for details. [c] Each ADF octahedral structure does not correspond to a minimum on the potential energy surface (i.e., ϕ and δ were fixed at 90.00°). [d] D_{3h} structure found at a minimum ∼6 kcal/mol lower than the O_h isomer. [e] The O_h isomer was not found at a minimum; its angles were fixed. [f] The D_{3h} isomer was not found at a minimum; its angles were fixed. [g] O_h structure found at a minimum ∼6 kcal/mol lower than the D_{3h} isomer, which was not found to be a minimum.

The electronic preference of $Ta(C{\equiv}CSi^tBu_3)_6^-$ for trigonal prismatic geometry is tempered somewhat by steric interactions that are responsible for the twist distortion toward an octahedron. Zirconium and hafnium have larger covalent radii (1.45, 1.44 Å) than tantalum (1.34 Å);[35] thus $M(C{\equiv}CSi^tBu_3)_6^{2-}$ (M = Zr, Hf) are expected to be less influenced by steric interactions that favor octahedral over trigonal prismatic geometries, yet the former stereochemistry results. The $M(C{\equiv}CSi^tBu_3)_6^{2-}$ (M = Zr, Hf) octahedron must be a consequence of an electronic preference or a moderate steric preference that overcomes any minor electronic preference toward trigonal prismatic coordination. Assuming the former is operable, perhaps the structural discrepancy is a consequence of the net charge on each ion. Pauling's electroneutrality principle[31] implies that the charge is partially delocalized on the ligands, rather than residing completely on the metal center. The charge will reside mainly on the carbon of the ligands that is directly bonded to the metal. The ligands of $M(C{\equiv}CSi^tBu_3)_6^{2-}$ (M = Zr, Hf) presumably carry about twice the net negative charge of those on $Ta(C{\equiv}CSi^tBu_3)_6^-$ and will therefore have stronger repulsive interactions between ligands, despite the greater size of the group 4 dianion. Repulsive forces at the ligand core render a trigonal prism relatively less stable than an octahedron according to the tenets of VSEPR.[1]

(2) Density Functional Calculations. Density functional (ADF)[36−38] calculations were conducted on hypothetical $Ta(C{\equiv}CH)_6^-$ (**5′**) and $Zr(C{\equiv}CH)_6^{2-}$ (**6′**) anions, thereby modeling the transition metal centers of [K(crypt 2.2.2)][$Ta(C{\equiv}C{-}Si^tBu_3)_6$] (**5**) and $\{Li(^tBu_3SiC{\equiv}C)_3\}_2Zr$ (**6**), respectively. The latter was chosen to represent $M(C{\equiv}CSi^tBu_3)_6^{2-}$ (M = Zr, Hf) because Zr is slightly less electropositive than Hf and should have a greater tendency toward trigonal prismatic coordination on that basis.[2−4] Use of the parent acetylide in **5′** and **6′** obviates unnecessary calculational details and provides an assessment of geometry-determining electronic factors without the steric complications intrinsic to the $-C{\equiv}CSi^tBu_3$ ligands.

Before proceeding with an analysis of the D_3 $Ta(C{\equiv}CH)_6^-$ (**5′**), the vibrational frequencies were calculated and the possibility of D_3 **5′** being a local energy minimum rejected because several imaginary vibrational frequencies were calculated. Subsequent geometry optimizations of the D_3-optimized structure in C_1 symmetry did not lead to computationally significant changes in total energy (<0.1 kcal/mol) or geometry, indicating almost no curvature for the potential energy surface in the vicinity of the minimum obtained from geometry optimization in D_3 symmetry. It can be safely concluded that constraining **5′** to D_3 provides a reasonable model. In contrast, the O_h **5′** model definitely does not correspond to a local energy minimum, nor is it near one; hence the constrained octahedral geometry was optimized simply to provide an energetic comparison to the D_3 **5′** version.

The D_3 $Ta(C{\equiv}CH)_6^-$ (**5′**) model was found to be an appropriate fit to the anion of [K(crypt 2.2.2)][$Ta(C{\equiv}CSi^tBu_3)_6$] (**5**, Table 8). The rectangular and trigonal face angles of **5′** and **5** are within a few degrees of one another, the tantalum−carbon distance of 2.234 Å in **5′** is only ∼0.06 Å longer than observed in **5**, and its C≡C bond length is <0.01 Å longer than that experimentally observed. The differences may be partly ascribed to the disparate substituents, H vs Si^tBu_3, and subtle electronic factors stemming from the sterically induced, significant C_3 twist (18°) of **5**, which undoubtedly contributes greatly to the discrepancies in ∠TaCC.

The O_h $Zr(C{\equiv}CH)_6^{2-}$ (**6′**) model is less satisfactory in mimicking the metric parameters of $\{Li(^tBu_3SiC{\equiv}C)_3\}_2Zr$ (**6**), with a ∼0.13 Å longer d(Zr−C) and a ∼0.022 Å longer d(C≡C). O_h **6′** was not shown to exist as a minimum on the potential energy surface, nor was it near a minimum. A 58° twist about the C_3 axis was applied to the D_3-optimized **6′**, generating a trigonal antiprismatic configuration that is within a few degrees in ϕ (Figure 7) from an octahedron. Upon optimization, the D_3 **6′** structure was reproduced; O_h **6′** was not obtained. Note that the d(Zr−C) and d(C≡C) of D_3 **6′** are closer to the experimental parameters of octahedral $\{Li(^tBu_3SiC{\equiv}C)_3\}_2Zr$ (**6**), despite the incorrect geometry.

Tables 9 provides the total energies obtained for $Ta(C{\equiv}CH)_6^-$ (**5′**) and $Zr(C{\equiv}CH)_6^{2-}$ (**6′**) upon optimization in D_3 and O_h symmetries and deconstructs them into electrostatic, Pauli, and orbital contributions.[36−38] The trigonal prismatic geometry is favored over an antiprismatic or octahedral configuration by ∼23.4 kcal/mol in **5′** and by only ∼8.8 kcal/mol in **6′**. This is

(36) (a) Baerends, E. J.; Ros, P. *Int. J. Quantum Chem.* **1978**, *S12*, 169−190. (b) Baerends, E. J.; Ellis, D. E.; Ros, P. *Chem. Phys.* **1973**, *2*, 41−51. (c) Baerends, E. J.; Ros, P. *Chem. Phys.* **1975**, *8*, 412−418.

(37) Baerends, E. J.; Rozendaal, A. In *Quantum Chemistry: The Challenge of Transition Metals and Coordination Chemistry*; Vellard, A., Ed.; NATO ASI Series C, Vol. 176; Reidel: Boston, 1986; pp 159−177.

(38) (a) Ziegler, T. In *Metal−Ligand Interactions. From Atoms, to Clusters, to Surfaces*; Salalub, P. R., Russu, N., Eds.; NATO ASI Series C, Vol. 378, Klauser Academic: London, 1992; pp 367−396. (b) Ziegler, T.; Rauk, A. *Theor. Chim. Acta* **1977**, *46*, 1−10.

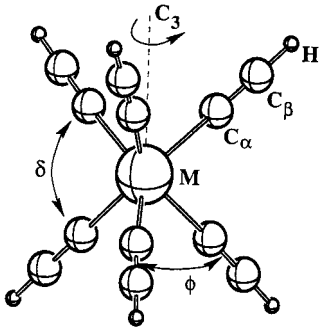

Figure 7. $M(C{\equiv}CH)_6^{n-}$ model and its parameters.

Table 9. Total Energy Deconstructions (kcal/mol) of D_3- and O_h-Optimized $Ta(C{\equiv}CH)_6^-$ (D_3 **5′**, O_h **5′**) and $Zr(C{\equiv}CH)_6^{2-}$ (D_3 **6′**, O_h **6′**)

optimized structure[a]	energy contributions			total energy
	electrostatic	Pauli	orbital	
D_3 **5′**	−2087.82	11 330.85	−12 098.74	−2855.06
O_h **5′**	−2024.06	11 125.41	−11 933.45	−2831.63
D_3 **6′**	−1913.26	10 814.35	−11 713.99	−2813.07
O_h **6′**	−1879.53	10 708.42	−11 632.98	−2804.24

[a] The octahedral structures do not correspond to minima on the potential energy surface.

Table 10. Calculated Hirshfeld Charges for D_3- and O_h-Optimized $Ta(C{\equiv}CH)_6^-$ (D_3 **5′**, O_h **5′**) and $Zr(C{\equiv}CH)_6^{2-}$ (D_3 **6′**, O_h **6′**)

optimized structure[a]	calculated Hirshfeld charges		
	metal	Cα	Cβ
D_3 **5′**	0.6266	−0.1668	−0.1551
O_h **5′**	0.6744	−0.1804	−0.1493
D_3 **6′**	0.5613	−0.2057	−0.2352
O_h **6′**	0.5928	−0.2161	−0.2308

[a] The octahedral structures do not correspond to minima on the potential energy surface.

the expected trend based on the greater HOMO/LUMO gap in the more electropositive, group 4 metal complex.[2] The electronic preference defined by summing the Pauli and orbital terms is best discussed in the context of LCAO MO calculations.[2] The sum of the Pauli term, essentially a measure of filled−filled orbital interactions, and the orbital term, a reflection of net-bonding interactions, favors octahedral over trigonal prismatic coordination in **5′** and **6′** by ∼40.2 and ∼24.9 kcal/mol, respectively. These terms are more than offset by electrostatic terms that favor the trigonal prisms of **5′** by ∼63.8 kcal/mol and D_3 **6′** by 33.7 kcal/mol. The latter component is a measure of the partitioning of charge within the complex and the sum of energies resulting from these interactions and should not be construed as representing the repulsive effects upon which the O_h preference in VSEPR is based.

The calculated Hirshfeld[39] charges for $Ta(C{\equiv}CH)_6^-$ (**5′**) and $Zr(C{\equiv}CH)_6^{2-}$ (**6′**) given in Table 10 indicate that M−Cα polarization manifests similar covalent bonding in both models, with a slightly greater polarization for zirconium in accord with its lower electronegativity and the greater charge of the dianion. While it is tempting to attribute the slightly greater length of the Cα≡Cβ bonds in **6′** (relative to **5′**) to polarization effects,[14] the subtle difference does not merit further scrutiny. As the charge on the complex ion is increased from **5′** to **6′**, Cβ accommodates a slightly greater percentage of negative charge, but the relatively even distribution of charge between Cα and Cβ strongly supports the contention that the acetylide ligands

(39) Hirshfeld, F. L. *Theor. Chim. Acta* **1977**, *44*, 129−138.

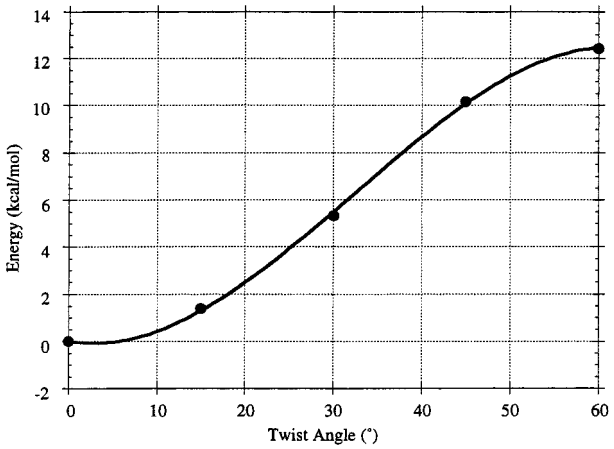

Figure 8. $Ta(C{\equiv}CH)_6^-$ (**5″**) twist angle (relative to optimized D_{3h} structure) vs energy. The bond lengths of D_{3h} **5″** were fixed and not optimized at each twist angle (see text).

are neither significant π-donors or -acceptors in either model. The periphery of **6′** obviously retains greater charge than the monoanion, **5′**; hence its interligand electrostatic repulsions are more significant.

In summary, the ADF calculations show a strong preference for the D_3 $Ta(C{\equiv}CH)_6^-$ (**5′**) over its octahedral counterpart in corroboration with the observed distorted trigonal prismatic geometry of $[K(crypt\ 2.2.2)][Ta(C{\equiv}CSi^tBu_3)_6]$ (**5**). A similar preference is observed for D_3 $Zr(C{\equiv}CH)_6^{2-}$ (**6′**), but it is substantially smaller; thus the observed octahedral geometry of $\{Li(^tBu_3SiC{\equiv}C)_3\}_2Zr$ (**6**) may be a consequence of interligand steric repulsions overcoming the D_3 electronic preference of the far less congested model.

(3) GAMESS Calculations. Table 8 lists structural parameters obtained from the geometry optimizations for $Ta(C{\equiv}CH)_6^-$ (**5″**) and $Zr(C{\equiv}CH)_6^{2-}$ (**6″**) conducted using GAMESS.[40−42] Aside from a significantly shorter *d*(TaCα) of 2.19 Å, which is very close to the experimentally observed 2.168 Å, the values are remarkably similar to those obtained from the ADF calculations.

Differences in the calculational models were revealed upon scrutinizing the energetics. D_{3h} $Ta(C{\equiv}CH)_6^-$ (**5″**) was found at a minimum on the potential energy surface, approximately 6 kcal/mol lower than O_h **5″**, which was determined not to exist at a minimum. While the GAMESS result mirrors the experimental and ADF preferences, the energetic disparity is rather small, especially in view of apparent steric influences that twist the tantalum center in $[K(crypt\ 2.2.2)][Ta(C{\equiv}CSi^tBu_3)_6]$ (**5**) away from a classical trigonal prism. To probe the effects of a twist, a crude calculation of the twist angle—relative to the optimized trigonal prism—versus energy was conducted (Figure 8). The calculations were done using fixed bond lengths (those of D_{3h} **5″**) and were not optimized at each twist angle; hence the energies are artificially high at large twist angles. Nonetheless, it is important to note that it is energetically easy to twist up to ∼20°, a value that apparently can mitigate any interligand steric repulsive effects, since the observed twist is ∼18° in **5**. It is plausible that the C_3 twist of the tantalum center in **5** can

(40) Schmidt, M. W.; Baldridge, K. K.; Boatz, J. A.; Elbert, S. T.; Gordon, M. S.; Jensen, J. H.; Koseki, S.; Matsunaga, N.; Nguyen, K. A.; Su, S. J.; Windus, T. L.; Dupuis, M.; Montgomery, J. A. *J. Comput. Chem.* **1993**, *14*, 1347−1363.

(41) (a) Krauss, M.; Stevens, W. J.; Basch, H.; Jasien, P. G. *Can. J. Chem.* **1992**, *70*, 612−630. (b) Stevens, W. J.; Basch, H.; Krauss, M. *J. Chem. Phys.* **1984**, *81*, 6026−6033.

(42) Cundari, T. R.; Gordon, M. S. *Coord. Chem. Rev.* **1996**, *147*, 87−115.

occur with negligible loss of electronic energy within the tantalum hexaacetylide core.

GAMESS predicts the structure of $Zr(C{\equiv}CH)_6^{2-}$ (**6″**) to be octahedral, in accord with the experimentally observed configuration of $\{Li(^tBu_3SiC{\equiv}C)_3\}_2Zr$ (**6**), but like the ADF calculations, d(Zr−C) is overestimated by about 0.10 Å. The octahedral preference is small—only ∼6 kcal/mol relative to D_{3h} **6″**, which was not found at a minimum but calculated as a stationary point.

A Mulliken population analysis performed to extract atomic charges for both $Ta(C{\equiv}CH)_6^-$ (**5″**) and $Zr(C{\equiv}CH)_6^{2-}$ (**6″**) implicated greater ionic character in the former; however, an alternative scheme by Löwdin suggested the opposite—the zirconium derivative displayed greater ionic character.[43] Instead of interpreting such approaches, the d(C≡C) of various XC≡CH was evaluated with the expectation of increasing distance with greater ionic character.[14] The following d(C≡C) were calculated: C_2H_2, 1.22 Å; HC_2Na, 1.25 Å; HC_2^-, 1.27 Å. Within this metrical context, the slightly longer d(C≡C) of O_h **6″** (1.24 Å) relative to that of D_{3h} **5″** (1.23 Å) supports the notion of a greater degree of ionic bonding in the zirconium case. Given the opposite predictions of the Mulliken and Löwdin analyses and the minor C−C bond distance difference of 0.01 Å, no definite answer can be reached regarding the relative ionic character of Ta vs Zr in the hexaacetylides, especially considering that there is no unique way to partition the total electron density within each molecule.

What then is the likely basis for the octahedral preference? Unlike in an extended Hückel molecular orbital approach, orbital information such as the energy of the HOMO/LUMO gap cannot be readily extracted when extended basis sets are employed. By using a configuration interaction−single (CIS) wave function, the energy between the ground and first excited states can be assessed and assumed to correlate with the HOMO/LUMO gap. The calculation suggests that the $t_{1u}-t_{2g}$ gap is much larger (∼6.5 eV) in the Zr dianion (**6″**) than the Ta anion (**5″**, ∼5.0 eV) in the O_h geometry, and also for the D_{3h} configurations, where the Zr gap is 7.5 vs 5.7 eV for Ta. From previous EHMO and ab initio calculations, as the HOMO/LUMO gap increases, the mixing of these orbitals is attenuated and the preference for trigonal prismatic coordination lessens.[2−4]

In summary, GAMESS correctly predicts the structural preferences for both $Ta(C{\equiv}CH)_6^-$ (**5″**) and $Zr(C{\equiv}CH)_6^{2-}$ (**6″**), although the magnitude of the energy difference between the O_h and D_{3h} configurations appears small. The shift to the octahedral geometry upon transitioning from Ta to Zr is rooted in an increase in the HOMO/LUMO gap for the latter, more electropositive group 4 element.

Conclusions

The extremely bulky $^tBu_3SiC{\equiv}C^-$ ligand has been used to circumvent synthetic difficulties in preparing homoleptic, d^0 early transition metal acetylide derivatives. Structural characterizations revealed a distorted trigonal prismatic (D_3) geometry for $(^tBu_3SiC{\equiv}C)_6Ta^-$ and an octahedral (O_h) configuration for $(^tBu_3SiC{\equiv}C)_6M^{2-}$ (M = Zr, Hf), where recent theoretical investigations suggest that a trigonal prismatic (D_{3h}) or C_{3v} arrangement should be preferred. Steric interactions of the $^tBu_3Si$ groups appear to cause the distortion from D_{3h} to D_3 in the tantalum case, while density functional (ADF) and effective core potential (GAMESS) calculations revealed a lessening preference for the trigonal prism upon shifting from Ta to Zr. Many factors contribute to the octahedral preference for $(^tBu_3SiC{\equiv}C)_6M^{2-}$ (M = Zr, Hf), including a minor steric perturbation. The most influential forces are the increased HOMO/LUMO gap in the zirconium—and presumably the Hf—dianion (relative to Ta), which mitigates against the second-order orbital mixing that renders a six-coordinate, d^0 species trigonal prismatic, and its increased peripheral charge. While the tenets of VSEPR suggest that interligand repulsions resulting from the charge on the acetylides is most important, neither calculation revealed such an emphasis, although the ionic character of $(^tBu_3SiC{\equiv}C)_6Zr^{2-}$ was tentatively assessed as greater than that of $(^tBu_3SiC{\equiv}C)_6Ta^-$.

Experimental Section

General Considerations. All manipulations were performed using either glovebox or high vacuum line techniques. Ethereal solvents were distilled from purple sodium benzophenone ketyl and vacuum transferred from the same immediately prior to use. Aromatic and aliphatic hydrocarbon solvents were distilled and vacuum transferred from sodium benzophenone ketyl with added tetraglyme (5 mL/L solvent) to solubilize the ketyl. Bis(trimethylsilyl)ether and dimethyl sulfoxide were dried over 4 Å molecular sieves. Benzene-d_6 (Cambridge Isotope Laboratories) was dried over sodium and then 4 Å molecular sieves and vacuum transferred and stored in the glovebox. THF-d_8 (Cambridge) was vacuum transferred from sodium benzophenone ketyl.

Sodium acetylide and potassium hydride were purchased from Aldrich as suspensions in xylenes/mineral oil and mineral oil, respectively, and were filtered, washed with hexane, and pumped to dryness. $ZrCl_4$, $HfCl_4$, and $TaCl_5$ were purchased from Strem and purified by sublimation (160−180 °C, 10^{-4} Torr). Crypt 2.2.2 and potassium triflate were purchased from Aldrich and used without further purification.

NMR spectra were obtained on Varian XL-200 (^{1}H) and XL-400 ($^{13}C\{^1H\}$) spectrometers. Chemical shifts are reported relative to the residual carbon or proton resonances of the solvent (benzene-d_6: ^{1}H, δ 7.15 ppm; ^{13}C, δ 128.39 ppm. THF-d_8: ^{1}H, δ 1.73 ppm; ^{13}C, δ 25.37). Infrared spectra were obtained with a Nicolet Impact 410 spectrometer interfaced with a Gateway 2000 computer.

Elemental analyses (EA) were performed by Oneida Research Services of Whitesboro, NY (C, H), and Robertson Microlit Labs of Madison, NJ (Li). The EA obtained for the transition metal alkynyl derivatives were obtained on crystalline samples checked by ^{1}H and $^{13}C\{^1H\}$ NMR spectroscopy and were found to be generally unsatisfactory. Potential problems include the sensitivity of the materials and their potential as sources of metal carbides.

Procedures. (1) Preparation of $^tBu_3SiC{\equiv}CH$. $^tBu_3SiBr$[25] (12.00 g, 43.0 mmol) was ground into a powder using a mortar and pestle and combined with NaC≡CH (3.00 g, 62.5 mmol) in a 250 mL flask attached to a 180° needle valve. Dry DMSO (75 mL) was added via syringe, and the suspension was stirred at 23 °C. Small aliquots were taken periodically and worked up following the procedure below. After 13 days the reaction was judged complete by a ^{1}H NMR spectrum of an aliquot, and the brown reaction mixture was emptied into a separatory funnel with 200 mL of hexane and 200 mL of water. The mixture was shaken vigorously, the organic phase collected, and the aqueous phase extracted with 100 mL more of hexane. The combined organic extracts were filtered through a plug of silica, and the hexane was removed. A ^{1}H NMR spectrum indicated a ∼8:1 molar ratio of $^tBu_3SiC{\equiv}CH$ to $^tBu_3SiC{\equiv}CSi^tBu_3$. The soft solid was partly dissolved in 150 mL of acetone and filtered, leaving most of the less soluble $^tBu_3SiC{\equiv}CSi^tBu_3$ behind. The solvent was removed and the solid slurried in an additional 30 mL of acetone and transferred to a sublimator, leaving behind more undissolved $^tBu_3SiC{\equiv}CSi^tBu_3$. Sublimation at 60 °C ($10^{-3}-10^{-4}$ Torr) to a dry ice/acetone coldfinger yielded 6.68 g of $^tBu_3SiC{\equiv}CH$ as a white solid containing ∼5% $^tBu_3SiBr$ by ^{1}H NMR analysis (69% yield).

(2) Preparation of $^tBu_3SiC{\equiv}CLi(OEt_2)_x$. To a 50 mL flask was added $^tBu_3SiC{\equiv}CH$ (1.50 g, 6.68 mmol) and 20 mL of diethyl ether via vacuum transfer. ^{n}BuLi (4.5 mL of a 1.6 M solution in hexane,

(43) Szabo, A.; Ostlund, N. S. *Modern Quantum Chemistry*; McGraw-Hill: New York, 1989; pp 149−152.

7.2 mmol) was added via syringe at ambient temperature. After stirring for 0.5 h, the product was crystallized from ether at −78 °C in two crops to yield 1.39 g of white, microcrystalline ^{t}Bu$_3$SiC≡CLi(OEt$_2$)$_x$ (x = 0.2 by ^{1}H NMR analysis, 73% yield). Anal. Calcd for ^{t}Bu$_3$SiC≡CLi(OEt$_2$)$_{0.2}$: C, 72.49; H, 11.92. Found: C, 72.02; H, 11.57.

(3) Preparation of ^{t}Bu$_3$SiC≡CK. ^{t}Bu$_3$SiC≡CH (500 mg, 2.23 mmol), KH (110 mg, 2.74 mmol), and 10 mL of THF were stirred in a flask for 12 h at 22 °C, and the volatiles were removed (a gas, presumably H_2, was present). The solid was filtered in ether and crystallized from ca. 7 mL at −78 °C to afford colorless ^{t}Bu$_3$SiC≡CK (418 mg, 71% yield).

(4) Preparation of {(THF)2Li(^{t}Bu$_3$SiC≡C)$_2$}Zr(C≡CSi^{t}Bu$_3$)$_3$(THF) (1). In a 50 mL flask were combined $ZrCl_4$ (100 mg, 0.429 mmol), ^{t}Bu$_3$SiC≡CLi(OEt$_2$)$_x$ (494 mg, 2.14 mmol), and 20 mL of THF. The solution was stirred overnight at ambient temperature, the volatiles were removed, and the mixture was filtered in ether. Two crystallizations from ether at −78 °C afforded 410 mg (67% yield) of colorless **1**. Anal. Calcd for $C_{82}H_{159}Si_5O_3ZrLi$: C, 68.79; H, 11.19; Li, 0.48. Found: C, 68.45; H, 10.95; Li, 0.41.

(5) Preparation of {(Et$_2$O)Li(^{t}Bu$_3$SiC≡C)$_2$}Hf(C≡CSi^{t}Bu$_3$)$_3$(OEt$_2$) (2). To a 50 mL flask containing $HfCl_4$ (50 mg, 0.16 mmol) and ^{t}Bu$_3$SiC≡CLi(OEt$_2$)$_x$ (200 mg, 0.794 mmol) was added 20 mL of ether at −78 °C. The reaction was slowly allowed to warm to 22 °C, where it was stirred for ∼12 h. Volatiles were removed from the reaction mixture, and the solid was triturated 3 times with ∼5 mL of hexanes. The product was dissolved in ether and filtered through a small plug of Celite. The salt cake was washed twice with ∼1 mL of ether, and the filtrate was placed in a −27 °C freezer. After 24 h, 60 mg (26%) of colorless crystals of **2** were isolated by filtration. Anal. Calcd for $C_{78}H_{155}Si_5O_2HfLi$: C, 64.57; H, 10.77. Found: C, 60.56; H, 10.25.

(6) Preparation of {Li(^{t}Bu$_3$SiC≡C)$_3$}Ta(C≡CSi^{t}Bu$_3$)$_3$ (3). $TaCl_5$ (200 mg, 0.558 mmol), ^{t}Bu$_3$SiC≡CLi(OEt$_2$)$_x$ (772 mg, 3.35 mmol), and 30 mL of benzene were stirred overnight in a 50 mL flask while being protected from light. After ∼12 h, the benzene was removed and ether was added. The suspension was filtered, and the LiCl was washed several times with ether. The product was collected as light-sensitive yellow microcrystals from ca. 12 mL of ether at −78 °C (563 mg, 68% yield). Anal. Calcd for $C_{84}H_{162}Si_6TaLi$: C, 66.00; H, 10.68; Li, 0.45. Found: C, 63.80; H, 10.36; Li, 0.42.

(7) Preparation of [K(crypt 2.2.2)][Ta(C≡CSi^{t}Bu$_3$)$_6$] (5). $TaCl_5$ (100 mg, 0.279 mmol) and ^{t}Bu$_3$SiC≡CLi(OEt$_2$)$_x$ (450 mg, ∼1.67 mmol) were stirred in benzene at 22 °C for 12 h. The solvent was removed, and potassium triflate (500 mg, 2.66 mmol) was added along with ∼25 mL of THF. The suspension was stirred for 16 h at 22 °C, the solvent was removed, and ∼25 mL of benzene was added. The yellow-brown suspension was filtered and the residual solid washed with benzene until all the yellow compound, presumably KTa(C≡CSi^{t}Bu$_3$)$_6$ (**4**), had been extracted. The benzene was removed, and crypt 2.2.2 (125 mg, 0.332 mmol) was added along with ∼25 mL of THF. The solution was stirred at 22 °C for 16 h, and the THF was removed. Ether (∼8 mL) was added to almost completely dissolve the solid, and hexane (∼8 mL) was added to precipitate a yellow solid, which was collected by filtration at 22 °C (430 mg, 75% yield). Anal. Calcd for $C_{102}H_{196}O_6N_2Si_6TaK$: C, 63.31; H, 10.21; N, 1.45. Found: C, 63.59; H, 10.00; N, 1.57.

(8) Preparation of {Li(^{t}Bu$_3$SiC≡C)$_3$}$_2$Zr (6). A bomb was charged with $ZrCl_4$ (92 mg, 0.40 mmol), ^{t}Bu$_3$SiC≡CLi(OEt$_2$)$_x$ (600 mg, 2.39 mmol), and ∼30 mL of benzene and heated at 80 °C for 12 h. The volatiles were removed, and the product was washed with ∼2 mL of hexanes. The salt cake was washed with ∼5 mL of ether and filtered. The filtrate was concentrated to ∼2 mL, and slow evaporation at 23 °C gave 95 mg (17%) of colorless, crystalline **6**. Anal. Calcd for $C_{84}H_{162}Si_6ZrLi_2$: C, 69.78; H, 11.29; Li, 0.96. Found: C, 68.08; H, 11.40; Li, 1.00.

(9) Preparation of {Li(^{t}Bu$_3$SiC≡C)$_3$}$_2$Hf (7). A bomb was charged with $HfCl_4$ (83 mg, 0.26 mmol), ^{t}Bu$_3$SiC≡CLi(OEt$_2$)$_x$ (400 mg, 1.59 mmol), and ∼30 mL of benzene and heated at 80 °C for 4 h. The volatiles were removed, and the white solid was dissolved in ∼4 mL of ether and filtered through a small plug of Celite. The solid was washed twice with 0.5 mL of ether, and slow evaporation at 23 °C gave 152 mg (38%) of colorless, crystalline **7**. Anal. Calcd for $C_{84}H_{162}Si_6HfLi_2$: C, 65.81; H, 10.65. Found: C, 64.04; H, 10.54.

Single Crystal X-ray Structural Investigations. (10) {(THF)$_2$Li(^{t}Bu$_3$SiC≡C)$_2$}Zr(C≡CSi^{t}Bu$_3$)$_3$(THF) (1). X-ray quality crystals were grown by slow cooling of an ether solution of **1** to −30 °C in a glovebox refrigerator. A colorless crystal was mounted in glass capillary for data collection at the Center for High Energy Synchrotron Studies (CHESS, A1 beam line). The crystal to detector distance was set at 43 mm, and a 2048 × 2048 pixel charge-coupled device was used to record the diffraction.[44] Data were collected as 7 s, 5° rotations, with a total of 360° collected. The first frame was indexed using the program DENZO,[45] yielding a triclinic unit cell given in Table 2. The remaining frames were indexed using DENZO, and all the data were scaled together with SCALEPACK. The structure was solved by direct methods (SHELXS), with hydrogen atoms introduced geometrically. Anisotropic thermal parameters were used for all non-hydrogen atoms.

11. {(Et$_2$O)Li(^{t}Bu$_3$SiC≡C)$_2$}Hf(C≡CSi^{t}Bu$_3$)$_3$(OEt$_2$) (2). X-ray quality crystals of **2** were grown by slow evaporation of an ether solution at −30 °C in a glovebox refrigerator (evaporation at 23 °C gave **7**). A colorless crystal was mounted in a glass capillary for data collection on a Siemens P4 diffractometer equipped with a SMART/CCD detector (Table 2). The structure was solved by direct methods (SHELXS). All non-hydrogen atoms were anisotropically refined, and hydrogen atoms were treated as idealized contributions.

(12) {Li(^{t}Bu$_3$SiC≡C)$_3$}Ta(C≡CSi^{t}Bu$_3$)$_3$ (3). X-ray quality crystals were grown by slow cooling of a hexane solution of **3** in a glovebox refrigerator set to −30 °C. Crystals were mounted in glass capillaries and protected from light during data collection on a Seimens P4 four-circle diffractometer (Table 2). The data were collected at 22 °C using a $\omega/2\theta$ scan with a variable speed of 1.5−29°/min. Two crystals were used to produce a complete data set—one (0.3 × 0.6 × 0.7 mm) for low-angle data and another (0.4 × 0.5 × 0.6 mm) for high-angle data. Lorentz, polarization, and empirical absorption corrections were applied. The structure was solved by direct methods (SHELXS), and hydrogen atoms were introduced geometrically. Anisotropic thermal parameters were used for all non-hydrogen atoms. The Ta atom was found on a *6a* special position (intersection of a 3-fold and a 2-fold axis). There is only one symmetry independent C≡CSi^{t}Bu$_3$ ligand in the structure. The Li cation was found on a *12c* special position (on a 3-fold axis). If the position was fully occupied, the Li:Ta ratio would be 2:1. To agree with elemental analysis, which indicated one Li per Ta, occupancy was set to 50%.

(13) X-ray Structure Determination of [K(crypt 2.2.2)][Ta(C≡CSi^{t}Bu$_3$)$_6$] (5). X-ray quality single crystals were grown by slow diffusion of hexane into a THF solution of **5** at 22 °C, while being protected from light. A suitable crystal was mounted in a thin-walled capillary and sealed under nitrogen. Data were collected on a Siemens P4 diffractometer equipped with a SMART/CCD detector. No evidence for symmetry higher than triclinic was found, and $P\bar{1}$ was used as the space group for the well-behaved refinement (Table 2). An empirical correction for absorption was applied to the data. All non-hydrogen atoms were anisotropically refined, and hydrogen atoms were treated as idealized contributions. In addition to the pair of ions, a diffusely formed and positionally disordered small molecule was located in an area remote from either ion at the inversion center. Since it forms a six-membered ring with bond parameters roughly in accord with benzene, it was treated as such, but the ring exists in a slight chair distortion and could also be the result of two superimposed orientations of THF. All computations used the SHELXTL (5.03) program library (G. Sheldrick, Siemens XRD, Madison, WI).

(14) {Li(^{t}Bu$_3$SiC≡C)$_3$}$_2$Zr (6). X-ray quality crystals of **6** were grown by slow evaporation at 22 °C of an ether/(TMS)$_2$O solution containing {(THF)$_2$Li(^{t}Bu$_3$SiC≡C)$_2$}Zr(C≡CSi^{t}Bu$_3$)$_3$(THF) (**1**). A suit-

(44) (a) Thiel, D. J.; Walter, R. L.; Ealick, S. E.; Bilderback, D. H.; Tate, M. W.; Gruner, S. M.; Eikenberry, E. F. *Rev. Sci. Instrum.* **1995**, *66*, 1477−79. (b) Walter, R. L.; Thiel, D. J.; Barna, S. L.; Tate, M. W.; Wall, M. E.; Eikenberry, E. F.; Gruner, S. M.; Ealick, S. E. *Structure* **1995**, *3*, 835−44.

(45) Otwinowski, Z. *DENZO*, a program for automatic evaluation of film densities; Department of Molecular Biophysics and Biochemistry, Yale University; New Haven, CT, 1988.

able crystal for single-crystal X-ray diffraction was selected and mounted in a nitrogen-flushed, thin-walled capillary. The data were collected on a Siemens P4 diffractometer equipped with a SMART/CCD detector. Systematic absences and the occurrence of equivalent reflections were consistent with the rhombohedral (indexed hexagonal) space groups, R3 and $R\bar{3}$. Chemical composition and the value of Z (=3) suggested the space group $R\bar{3}$, which yielded chemically reasonable and computationally stable results of refinement. The structure was solved by direct methods, completed by subsequent difference Fourier syntheses, and refined by full-matrix least-squares procedures. Further refinement of the crystal structure showed signs of merohedral twinning; a [b, a, $-c$] transformation matrix was applied to resolve the twinning which decreased the R factor from ~17% to ~5%. No absorption corrections were required because there was less than 10% variation in the integrated ψ-scan intensity data. The dianion lies on a 3-fold axis and an inversion center. The unique lithium cation lies on a 3-fold axis. All non-hydrogen atoms were refined with anisotropic displacement parameters, and hydrogen atoms were treated as idealized contributions. All software and sources of the scattering factors are contained in the SHELXTL (5.03) program library (G. Sheldrick, Siemens XRD, Madison, WI).

(15) {Li(^{t}Bu$_3$SiC≡C)$_3$}$_2$Hf (7). X-ray quality crystals of **7** were grown by slow evaporation at 22 °C of an ether solution (evaporation at −30 °C yielded **2**). A suitable crystal for single-crystal X-ray diffraction was selected and mounted in a nitrogen-flushed, thin-walled capillary. The data were collected on a Siemens P4 diffractometer equipped with a SMART/CCD detector. Systematic absences and the occurrence of equivalent reflections were consistent with the rhombohedral (indexed hexagonal) space groups, R3 and $R\bar{3}$. Chemical composition and the value of Z (=3) suggested the space group $R\bar{3}$, which yielded chemically reasonable and computationally stable results of refinement. An empirical absorption correction was applied to the data. The structure was solved by direct methods (SHELXS). The dianion lies on a 3-fold axis and an inversion center, and the unique lithium cation lies on a 3-fold axis. All non-hydrogen atoms were refined with anisotropic displacement parameters, and hydrogen atoms were treated as idealized contributions.

Calculations. (16) Density Functional Calculations. All Amsterdam functional (ADF, release 2.0.1) calculations[36−38] were conducted using the Vosko, Wilk, and Nusair[46] parametrization of the local density approximation (LDA) to the exchange and correlation functional. The gradient corrections of Becke[47,48] (exchange) and Perdew[49] (correlation) were included in the exchange-correlation functional.

The Slater-type orbital (STO) basis sets employed for Ta, Zr, C, and H were all of triple-ζ quality with a single polarization function added for C and H (atom database IV in ADF). All electrons up to and including the 5p shell for Ta, the 4p shell for Zr, and the 1s shell for C were treated within the framework of the frozen core approximation.

The numerical integration scheme in ADF was set to provide not less than 5 decimal places of accuracy when energy gradients were computed.

(17) GAMESS. The Hartree−Fock calculations reported herein utilize the GAMESS[40] program in parallel and serial mode. All molecules studied computationally are closed-shell singlets. Geometries are fully optimized within the limitations of the point group symmetry indicated. The energy Hessian is calculated at all stationary points to characterize them as minima (zero imaginary frequencies), transition states (one imaginary frequency), or higher order saddle points.

All calculations employ the effective core potentials of Stevens et al. for zirconium, tantalum, and carbon and the -31G basis set for hydrogen atoms.[41] The zirconium, tantalum, and carbon atoms have 18, 60, and 2 electron cores, respectively.[41] The transition metal valence basis sets (VBSs) are quadruple and triple-ζ for the sp and d manifolds, respectively. The oxygen VBS is double-ζ-plus-polarization. The Stevens ECP/VBS scheme has been widely employed in numerous studies and has been found to yield accurate prediction of metric, energetic, and spectroscopic data for d-block complexes in a diverse array of chemical environments.[42]

Acknowledgment. We thank the National Science Foundation (T.P.V., Inorganic Materials Trainee; P.T.W., Grant CHE-9528914; T.R.C., Grant CHE-9614346) and Cornell University for support of this research.

Supporting Information Available: Tables listing of a summary of crystal data encompassing data collection and solution/refinement, atomic coordinates, isotropic and anisotropic temperature factors, hydrogen atom coordinates, bond lengths, and bond angles of {(THF)$_2$Li(^{t}Bu$_3$SiC≡C)$_2$}Zr(C≡CSi^{t}Bu$_3$)$_3$(THF) (**1**), {(Et$_2$O)Li(^{t}Bu$_3$SiC≡C)$_2$}Hf(C≡CSi^{t}Bu$_3$)$_3$-(OEt$_2$) (**2**), {Li(^{t}Bu$_3$SiC≡C)$_3$}Ta(C≡CSi^{t}Bu$_3$)$_3$ (**3**), [K(crypt 2.2.2)][Ta(C≡CSi^{t}Bu$_3$)$_6$] (**5**), {Li(^{t}Bu$_3$SiC≡C)$_3$}$_2$Zr (**6**) and {Li-(^{t}Bu$_3$SiC≡C)$_3$}$_2$Hf (**7**) (51 pages, print/PDF). See any current masthead page for ordering information and Web access instructions.

JA9802899

(46) Vosko, S. H.; Wilk, L.; Nusair, M. *Can. J. Phys.* **1980**, *58*, 1200−1211.
(47) Becke, A. D. *J. Chem. Phys.* **1986**, *84*, 4524−4529.
(48) Becke, A. D. *Phys. Rev. A* **1988**, *38*, 3098−3100.
(49) (a) Perdew, J. P. *Phys. Rev. B* **1986**, *33*, 8822−8824. (b) Perdew, J. P. *Phys. Rev. B* **1986**, *34*, 7406.